Technical Note

1966-59

G. Ploussios

Noise Temperature of Airborne Antennas at UHF

6 December 1966

Prepared under Electronic Systems Division Contract AF 19(628)-5167 by

Lincoln Laboratory

MASSACHUSETTS INSTITUTE OF TECHNOLOGY

Lexington, Massachusetts

The work reported in this document was performed at Lincoln Laboratory, a center for research operated by Massachusetts Institute of Technology, with the support of the U.S. Air Force under Contract AF 19(628)-5167.

MASSACHUSETTS INSTITUTE OF TECHNOLOGY
LINCOLN LABORATORY

NOISE TEMPERATURE OF AIRBORNE ANTENNAS AT UHF

G. PLOUSSIOS

Group 62

TECHNICAL NOTE 1966-59

6 DECEMBER 1966

LEXINGTON MASSACHUSETTS

ABSTRACT

Partial results of an experimental program to determine the electromagnetic noise environment at UHF on board an aircraft are presented. Contributors to an airborne receiver noise temperature including galactic noise, earth temperature, P-static, atmospherics and industrial noise were measured and are discussed. A model of the industrial noise is presented whereby the industrial area is considered as a uniformly distributed source of independent radiators, the magnitude being the same for all cities measured with the exception of the New York City area.

RFI generated by on-board equipment and/or ground transmitters will be covered in a subsequent report.

Accepted for the Air Force
Franklin C. Hudson
Chief, Lincoln Laboratory Office

NOISE TEMPERATURE OF AIRBORNE ANTENNAS AT UHF

I. INTRODUCTION

The noise level of an airborne UHF receiver is ultimately limited by the receive antenna temperature. In order to characterize this limit a three-part experimental program was initiated. The first two portions of the program provided the necessary data to describe continuous and transient noise levels inherent to an airborne system. The third portion of the program (still in progress), deals with man-made coherent radiation. This source of noise will be covered in a subsequent report.

Electromagnetic radiation originating from the earth, atmosphere and galaxy all contribute to the antenna temperature, the relative importance of each source being dependent upon antenna illumination. Equivalent expressions for determining antenna temperature, using the radio astronomers' terminology, are shown below.

$$T_a = \frac{G_o}{4\pi} \sum_i T_{B_i} D(\Omega_i) \qquad (1)$$

where:

T_a = antenna terminal temperature due to noise sources external to the antenna

T_{B_i} = brightness temperature in solid angle Ω_i

$D(\Omega_i)$ = normalized receive antenna radiation pattern over solid angle Ω_i

G_o = antenna gain

$$T_a = \frac{G_o}{4\pi} \int_0^{2\pi} \int_{-\pi/2}^{\pi/2} T_B(\theta, \phi)\, D(\theta, \phi) \cos\theta \, d\theta \, d\phi \qquad (2)$$

where $T_B(\theta, \phi)$ = Brightness temperature as a function of the spherical co-ordinates θ and ϕ

$D(\theta, \phi)$ = normalized receive antenna radiation pattern

θ = elevation angle measured from the horizon.

In the following sections measured values of the brightness temperature of the various sources illuminated by the receive antenna are presented. The frequency, time and geographical dependence of these sources are discussed. In addition, equations and curves are derived relating the effect of noise generated in industrial areas, city noise, on the receive antenna temperature.

Data was taken at three frequencies, 226.2 MHz, 305.5 MHz and 369.2 MHz using total power radiometers, each with a 1.2 MHz bandwidth and 2 msec integration. A C-135 jet aircraft and a C-131 propeller type aircraft were the test vehicles. A UHF blade (monopole) antenna, the AT/256, mounted on the top of the fuselage was used on the C-135. This antenna produced primarily overhead coverage. On the C-131 a 2-dipole array and reflector was mounted under the aircraft fuselage resulting in downward illumination with an average beamwidth of 42° x 112°. A more detailed description of the measurement equipment used is described in the appendix.

II. BACKGROUND EARTH AND GALACTIC NOISE

Galactic noise temperature in the UHF range varies as λ^{α}, where, depending upon the galactic model chosen,[1] α falls between 2.5 and 2.85. The temperature of an antenna with a hemispherical radiation pattern looking skyward was computed using Eq. (1) and the published radio map of the galaxy at 250 MHz.[2] The result is shown in Fig. 1, where the two curves shown correspond to hemispheres including the galactic center and galactic pole respectively. A wavelength relationship of $\lambda^{2.6}$ was used in computing the curves.

The effect on antenna temperature, due to the sun, was not included in Fig. 1, but should be of secondary importance under almost all conditions.

The brightness temperature of the quiet sun is proportional to λ with a temperature of 7×10^5 °K at 300 MHz[3]. The arc subtended by the sun is approximately 1/2°. In the case of an antenna with a hemispherical radiation pattern the effect of the sun, using Eqs. (1) or (2), is to raise its temperature 7°K at 300 MHz. Therefore, only during severe periods of solar activity will the sun cause a significant change in the receive antenna temperature of a low gain antenna. The sun's contribution is proportional to the receive antenna gain and therefore becomes significant as the antenna gain is increased.

Measurements taken on the C-135 over the Atlantic ocean with the upward looking blade antenna resulted in antenna temperatures of approximately 150°K at all three frequencies. These values have not been corrected to remove the effects due to transmission line loss (1/2 to 1 db), antenna efficiency, antenna VSWR, and contribution due to the ocean illuminated (approximately 20% of the antenna radiation pattern is below the horizon). Not having accurate information on the antenna radiation pattern or efficiency, no accurate evaluation of the galactic temperature is possible. However, all the above factors add to the measured antenna temperature with the greatest amount added at 369 MHz due to the higher transmission line loss. This would indicate galactic temperatures of less than 150°K with lower temperatures at the high end of the UHF band, i.e., results in general agreement with the curves of Fig. 1.

The brightness temperature of the earth is a function of the terrain being observed. It consists of thermal radiation from the earth plus reflected galactic noise.[1,4] The temperature over ocean has been measured at 2 GHz to be considerably lower than that over land,[1] with the latter being 300°K. Data taken on the C-131 (downward looking antenna) indicated antenna temperatures of 250 to 300°K over rural land and 160°K over the Atlantic ocean at the three test frequencies.

III. ATMOSPHERICS

Excessive noise levels due to atmospherics is a common problem at HF and lower frequencies. Since the energy radiated by a lightning discharge

drops off rapidly as frequency is increased and since propagation at UHF is primarily "line-of-site", this source of noise has not been a problem with most of the existent UHF communications equipment, which have relatively low sensitivity receivers compared to standards of today.

A great deal of research has gone into determining the nature of a thunderstorm and trying to obtain an accurate model of this phenomenon. Most of the experimental work has been done at frequencies below 100 kc with little published data above 100 MHz known to the author.

It has been estimated that there are 2000 thunderstorms in progress around the earth at any one time producing 100 lightning strokes/sec.[5] The peak thunderstorm activity occurs over tropical land masses during daylight hours. Thunderstorm distribution as a function of time and geography is available in the published literature.[5]

Each lightning discharge consists of a leader stroke (low rf energy content) from a cloud to ground (or clouds) plus at least one return stroke (high energy content) from the ground. A typical lightning flash has more than one return stroke, 4, being the typical number. The average duration of the stroke is 1/5 to 1/4 seconds. Horner[6] has calculated typical radiated power levels for a number of frequencies. These values are plotted in Fig. 2. The values in this figure represent the mean power level radiated over a 200 m sec. period, which he assumed to be the duration of the flash. Peak power levels were estimated by Horner to be 13 db higher than the mean at 100 mc.

The mean power level over the frequency spectrum (Fig. 2) is roughly proportional to λ^2 with a higher rate at frequencies above 10 MHz. Table I contains the expected flux (power) density, S_ν, and antenna temperatures expected based upon the curve in Fig. 2 and the assumption of unity antenna gain in the direction of discharge. Experimental data obtained on the KC-135 when flying at an altitude of 35K ft. within a range of 1 to 10 miles of a thunderhead between Nassau and Puerto Rico has been examined with typical results listed in the same table. Horner assumes that the phase center

of a lightning discharge occurs at an altitude of between 1 to 2 km which would put it well below the horizon of the test antenna used. Since the blade antenna does give appreciable below horizon coverage, any loss in gain in the direction of the discharge should be nominal. The 6 to 30 db lower temperatures measured than that predicted from extrapolating Horner's data is therefore not simply due to antenna pattern discrimination. An additional column of data is shown in Table I corresponding to typical mean temperatures measured the same day while the aircraft was on the ground in Puerto Rico. The storm during this measurement was approximately 15 miles distant. The receive antenna gain in the direction of the storm was between 1-1/2 and 3 db which again indicates lower levels than expected, in this case 6 to 10 db low. The data discussed above was obtained from discharges produced in single storm cells. Additional data was recorded the next day over the ocean while passing through lightning storms in a frontal system with results which were essentially the same.

Typical radiometer waveforms recorded while passing within a 10 mi. range of a storm cell are shown in Figs. 3 and 4. The repetition rate of the bursts were in the order of 20/min., where a burst was counted if it lasted $> 1/8$ second, was discernible on all three channels and was separated by at least 1 second from an adjacent burst. This rate is much higher than predicted.[6] Indeed, if all bursts present are counted the interference rate is even greater. This is illustrated in Fig. 5.

IV. PRECIPITATION STATIC

Precipitation static (P-static) occurs when there is a discharge of the potential developed on the aircraft surface when flying through precipitation and/or clouds. Nanevicz and Tanner pointed out that the P-static noise level at the terminals of an airborne antenna is a function of the type antenna used, the location on the aircraft, the specific aircraft and the type and condition of the static discharges used.[7,8] The noise level associated with this discharge drops off rapidly with increasing frequency, Nanevicz and Tanner having studied the effect up to 20 MHz. The effects due to P-static have been observed as high as 136 MHz by Bendix[9] during test flights on a Boeing 707. In fact,

TABLE I

Mean Power Density and Temperature Due to Lightning Discharge

Range / Freq.	S_ν (w/m^2/Hz) 10 mi.	S_ν (w/m^2/Hz) 1 mi.	Expected T ($^\circ$K) 10 mi.	Expected T ($^\circ$K) 1 mi.	Measured T($^\circ$K) In Air 1-10 mi.	Measured T($^\circ$K) On Grnd. 15 mi.
226.2 MHz	1.2×10^{-19}	1.2×10^{-17}	6.3×10^{4}	6.3×10^{6}	5×10^{3}	4.1×10^{3}
305.5 MHz	1.9×10^{-20}	1.9×10^{-18}	1.6×10^{4}	1.6×10^{6}	2.3×10^{3}	2.6×10^{3}
369.2 MHz	4.8×10^{-21}	4.8×10^{-19}	6.6×10^{3}	6.6×10^{5}	1.5×10^{3}	1.4×10^{3}

Bendix observed temperatures in excess of 200,000°K at the test frequencies during P-static conditions. This level, however, was due to static discharge from the test antenna (blade type) pointing out the importance of P-static consideration in the design and installation of an aircraft antenna.

Several flights on both the C-135 and C-131 were made under conditions conducive to P-static. On the C-135 no increase in noise level was measured during any of these flights. However, P-static was measured on several occasions on the C-131. Figure 6 shows the noise level at the 3 test frequencies during a typical period of P-static. Typical pulse magnitude ranged from 1500°K - 3000°K at 226.2 MHz (-137 dbm/kHz to -134 dbm/kHz) to 500° - 1000°K at 305.5 MHz (-141.5 dbm/kHz to -138 dbm/kHz) and less than 500°K at 369 MHz.

The reason for the different results on the two aircraft is attributed to the different static dischargers used. On the C-135 the ortho-decoupled dischargers described by Nanevicz and Tanner are used whereas the C-131 had the older wick-type discharger (AN/ASA-3).

V. NOISE RADIATED BY CITIES

Noise generated in industrial areas is considered to fall under the category of coherent or incoherent noise. Coherent sources include radiation from communication equipment, radar, navigational aids, etc. These sources, classified under the broader title of RFI, vary with geography and frequency band and will not be discussed below. Incoherent man-made noise is primarily generated by ignition systems, both mobile and stationary, power lines and other electrical machinery. This energy, which is impulsive in character, is the subject of this section.

During the past 15 years a number of investigators have made noise measurements on the ground in urban and suburban areas. The most comprehensive survey of this data covering 14 years of measurements by a number of different organizations was made by Skomal.[10] This data along with recent data collected for the FCC[11] is particularly geared for use in mobile and ground receiver system design. Use of this data, therefore, to determine expected antenna temperatures of an airborne system in the vicinity of an industrial area is questionable.

On the ground and at low altitudes the spectrum of man-made noise appears to contain large numbers of discrete lines. At higher altitudes, i.e., as the number of sources illuminated per solid angle increases, the noise would be expected to approach white noise. This is indeed what was observed when flying at altitudes greater than 5000 feet and correspondingly illuminating city areas greater than 3 sq. miles. The analysis below is based on the assumption that we are dealing with white noise at the receiver, and therefore with antenna systems that illuminate industrial areas of at least 3 sq. miles.

Analysis

The analysis models the industrial area as a radiating aperture consisting of a large number of statistically independent point sources. The effective ground power density is computed based upon measurements taken over a number of cities and is shown to be constant within $\pm$ 1 db over the length of the city with little difference in magnitude from city to city (with one exception). Equations relating this model of an industrial area to the effective receive antenna temperature are presented.

The general Eqs. (1) and (2) for antenna temperature can be used if values of $T_B(\theta, \phi)$ can be determined. Upon examining the geometry, however, it becomes apparent that the more fundamental and useful quantity is $C(\theta, \phi)$, the power density along the ground in watts/m^2/Hz. Assuming the city to be made up of a large number of statistically independent radiators the received power level would be the summation of the received power levels from the individual sources. Defining a ground power density $C(\theta, \phi)$ the received power would be (see Fig. 7).

$$P_r = \frac{\lambda^2}{16\pi^2} B G_o \int \int D(\theta, \phi) \frac{G_t C(\theta, \phi)\, dA}{\rho^2}$$

Substituting for the incremental area, dA, of Fig. 7 we get

$$P_r = kT_a B = \frac{\lambda^2 B G_o}{16\pi^2} \int_0^{2\pi} \int_{-\pi/2}^{\pi/2} D(\theta, \phi)\, C(\theta, \phi)\, G_t(\theta, \phi) \frac{\cos\theta}{\sin\theta} d\theta d\phi \quad (3)$$

where k = Boltzman's constant = 1.38×10^{-23}

$G_t(\theta, \phi)$ = effective radiation pattern of the earth generated radiation

B = bandwidth of receiver

Due to the randomness of the energy source we can assume $G_t(\theta, \phi)$ to be independent of ϕ and therefore equal to $G_t(\theta)$. Comparing Eq. (3) with (2) we get for $T_B(\theta, \phi)$.

$$T_B(\theta, \phi) = \frac{\lambda^2 G_t(\theta)\, C(\theta, \phi)}{4\pi k \sin\theta} \quad (4)$$

The above equation points out the dependence of T_B on θ and demonstrates the fundamental nature of $C(\theta, \phi)$. The one disconcerting item in Eqs. (3) and (4) is that T_B and consequently T_a approaches infinity as θ approaches zero if $G_t(\theta)\ C\ (\theta, \phi)$ does not approach zero faster than $\sin\theta$. In fact, θ never reaches zero when dealing with a spherical earth and $C(\theta, \phi)$ is non-zero for only limited ranges of θ.

As the distance from the industrial area becomes large (see Fig. 8) we get:

$$T_a = \frac{\lambda^2}{16\pi^2 k} D(\theta_o, \phi_o)\ C\ (\theta_o, \phi_o)\ G_t(\theta) G_o\ \frac{\cos\theta}{\sin\theta}\ \Delta\theta\ \Delta\phi \qquad (5)$$

where:

$$\Delta\theta = \theta_2 - \theta_1 = \frac{b \sin\theta_o}{\rho}$$

$$\Delta\theta = \phi_2 - \phi_1 = \frac{a}{\rho \cos\theta_o}$$

$$T_a = \frac{\lambda^2 G_o\ D(\theta_o, \phi_o)\ G_t(\theta_o)\ C\ (\theta_o, \phi_o)\ ab}{16\pi^2 k \rho^2}$$

$$= \frac{P_t G_t(\theta_o) G_o D(\theta_o, \phi_o)\ \lambda^2}{16\pi^2 k \rho^2} \qquad (6)$$

which is the standard energy transfer equation for a point source of power $P_t = C(\theta_o, \phi_o)\ ab$.

Experimental Results

A large number of test runs (approximately 50 flight hours were logged) were made over East coast cities at different altitudes, in an effort to determine noise distribution over cities, noise level differences between cities, differences due to time of day and year, and frequency dependence. A major problem was to distinguish background noise radiated from coherent interfering signals, RFI. With the aid of a tunable wide band receiver and spectral display it is believed that most of the interfering signals have been discounted in the following analysis.

Data runs were taken at altitudes of 2000 ft. to 19,000 ft. The runs were misleading at 2000 ft. since the receive noise was definitely not white

gaussian. An example of this is shown in Fig. 9 where radiometer data taken at 2000 ft. over a major highway (Rte. 128 north of Boston) clearly shows the impulse noise characteristic of auto ignition. In addition the frequency dependence and magnitude of the noise level recorded were not consistent with data taken at higher altitudes during the same day, the results indicating that we were not always in the far field of the radiators on the ground. At altitudes of greater than 5000 ft. the results were consistent, and consequently, the data from these altitudes will be the only ones considered in the following analysis.

Defining the boundaries of a city is subjective. Skomal and other have taken measurements in areas they define as Urban and Suburban. They have found that Suburban noise levels, on the ground, run 10 db or lower than that in Urban areas. In the analysis we consider the Urban area only. The effect of Suburban areas can be computed separately, but in any case will have only a secondary effect on the resultant antenna temperature.

The Miami Urban area was chosen as an excellent area to map since it has well-defined boundaries. On the East it is bordered by ocean and on the West by swamp. A number of runs were made over the area. The angular sector that the city metropolitan area occupies, as seen from the aircraft during one of the test runs at 18,000 ft. is shown in Fig. 10. A noise density profile can be computed assuming an average $C(\theta, \phi)$ over the portion illuminated at any one time and $G_t(\theta) = 1$. Then:

$$T_a = \frac{\lambda^2 C_x}{16 \pi^2 k} \; G_o \; I_x \qquad (7)$$

where C_x = power density along the length of the city and

$$I_x = \frac{1}{2}\left[I_+ + I_-\right]$$

$$I_+ = \int_0^{2\pi} \int_{\theta_1}^{\pi/2} D(\theta, \phi)\, \cot\theta\, d\theta\, d\phi$$

$$I_- = \int_0^{2\pi} \int_{\theta_2}^{\pi/2} D(\theta, \phi)\, \cot\theta\, d\theta\, \phi \qquad (8)$$

Since $D(\theta, \phi)$ is symmetrical about $\theta = \frac{\pi}{2}$, $I_+ = I_-$ when $\theta_1 = \theta_2 = \theta_\ell$. The function $I(\psi)$, where $\psi = \frac{\pi}{2} - \theta_\ell$, is evaluated in Appendix B based upon the test antenna pattern. The function is plotted in Fig. 11.

Using data taken at 18,000 ft. over Miami, an antenna gain of 9 db, Figs. 10 and 11, and Eq. (7), C_x was computed and is plotted in Fig. 12. With the exception of the northern edge of the city (where the illumination of Hollywood was present in the data, but not included in the outline of the city shown in Fig. 15) the value computed for C_x is constant over the city within $\pm$ 1 db. The mean value of C_x between x = 4 mi. and 18 mi. is shown in Fig. 12 and is used to compute in reverse the expected antenna temperature of the test antenna. This is shown in Fig. 13 along with the measured data.

It is of interest to note that the data used above was taken Wednesday, Nov. 17, 1965 at 1:30 P.M. local time and that a second set of data taken over identical runs Wednesday, Feb. 23, 1966 resulted in uniformly higher noise temperatures on all three channels in the order of 3 db. On no corresponding set of data runs over other cities did we note a difference in noise temperatures approaching 3 db. The implication clearly is that the Florida tourist season has a definite effect upon the UHF noise level.

An additional bit of information that can be computed from the Miami data runs is the total power radiated from the city. Based upon an average calculated C_x and an estimated Urban area of 117 sq. mi. the total power radiated (linear polarization) is .46 mw/MHz at 305.5 MHz during the tourist season and half that during the "off" season. At 226.2 MHz a similar estimation of C_x by comparing relative noise temperatures results in noise power

of .72 mw/MHz and .36 mw/MHz. Interference on the 369.2 MHz channel prevented any estimation of C at this frequency over Miami.

Miami is not unique in having an effective uniform power density distribution when areas >3 sq. mi. are illuminated. Flying at altitudes of 8000 ft. or greater over large cities such as New York and Philadelphia resulted in near constant antenna noise temperature over the city length. Since the corresponding city half angle, ψ_o, over the length of these cities was $>60^o$ and therefore $I(\psi)$ nearly constant the conclusion can be made that C_x is also constant. This is illustrated in Fig. 14 in the case of Philadelphia. In this case the aircraft was flown at an altitude of 18,000 ft. over the center of the city, starting south of the city and traveling north, north-east over Broad Street to a point between the Johnsville NAF and Willow Grove NAS. When flying at low altitudes greater detail of the power distribution becomes apparent as is shown in Fig. 15.

Table II lists the noise temperature levels, T_a, measured over the center of a number of U.S. cities. As seen from this table the only metropolitan area that resulted in appreciably higher temperatures is New York. The temperature levels recorded over Orlando and Jacksonville are lower than the other cities listed due to the smaller angular sector these cities occupied. To determine the average C_x of these cities the city limits would have to be determined in order to compute the illumination angle ψ_o and therefore I_x. However, it is seen from Fig. 11 that I_x saturates for illumination angles in excess of 60^o. With the exception of Jacksonville and Orlando all the data listed in Table II was obtained when ψ_o was very near 60^o or greater. Therefore the value of C_x for these cities is proportional to the listed temperatures. In the case of Jacksonville and Orlando the illumination angle was substantially less than 60^o and therefore the corresponding I_x was lower. This accounts for the lower temperatures listed for these two cities.

Data was taken during one night flight over the east coast cities. Unfortunately the weather was poor during this flight resulting in poor visibility and P-static and consequently limiting the quantity and accuracy of the data. However, the data did indicate a lower temperature level over the Baltimore-

Philadelphia-New York area. The levels were 3 to 7 db lower than previous measurements made during normal working hours. These measurements were taken between midnight and 2 A. M.

The frequency dependence of the noise temperature over a large number of independent measurements was determined by selecting data points from

TABLE II

Noise Temperature Recorded on C-131 Over Eastern U.S. Cities

City		Altitude (Ft.)	Temperature (^{o}K) 226.2 MHz	305.5 MHz	369.2 MHz
Boston		8K	22,000	8,000	*
Baltimore		18K	23,000	7,000	*
Jacksonville		14K	14,000	3,400	*
Miami	(Cold)	18K	14,000	4,600	*
	(Hot)	10K-18K	27,000	10,500	*
Orlando		9K	9,000	4,000	2,200
Philadelphia		8K-18K	26,000	9,000	6,000
Brooklyn		8K-18K	60,000	19,000	9,500
Manhattan		8K-18K	75,000	30,000	16,000

*Accurate values not obtained due to ground RFI.

data runs at altitudes of 7.5 K ft. and higher over all of the cities checked. Points on the same run were chosen, separated sufficiently in time, to prevent overlap of ground illumination. The ratio of the temperatures recorded at each data point was computed and averaged. The result is:

$$\frac{T_a \text{ @ } 305.5 \text{ MHz}}{T_a \text{ @ } 226.2 \text{ MHz}} = .31 \qquad (9)$$

$$\frac{T_a \text{ @ } 369.2 \text{ MHz}}{T_a \text{ @ } 226.2 \text{ MHz}} = .18 \qquad (10)$$

A total of 81 and 40 independent points were used in computing the ratios of Eqs. (9) and (10) respectively.

In order to obtain a comparable relationship between the values of C_x at the three test frequencies a relationship between the products $G_o I_x$ at the three frequencies must be determined. The data points chosen in evaluating Eqs. (9) and (10) corresponded to points where $\psi_o = \frac{\pi}{4} \pm 20^o$. At $\psi_o = 45^o$, $I(\psi)$ at 369.2 MHz is 1.6 db greater then $I(\psi)$ at the two lower frequencies. However the antenna gain G_o at 369.2 MHz is 1-1/2 db lower than that at the lower two frequencies. The product $G_o I_x$ is therefore essentially the same at all three frequencies at $\psi_o = 45^o$ and will furthermore be assumed identical for all the data points chosen. The values of C vs frequency are plotted in Fig. 16 using the C_x computed for a "hot" Miami at 305.5 MHz and Eqs. (7) and (9) and (10). Along with this data the often used values for Urban noise published in the ITT handbook[12] and converted to the same units is also plotted. It is interesting to note that the average slope of the two curves is similar but that the levels differ by 12.5 to 14.5 db. The difference in magnitude is not surprising since the quantity being measured is not actually the same, the ITT data representing the noise density experienced by a receiver on the ground in the Urban area, in the middle of the random radiating sources. Whereas C_x represents the effective noise density of the skyward radiated power.

Antenna System Temperature

To determine analytically the effect of a city on the temperature of an airborne antenna is a laborious procedure if one were to use Eq. (3) directly. There are a couple of ways of circumventing this lengthy calculation however.

If the distance between the aircraft and the city is greater than the largest dimension of the city and if the illumination pattern over the city is fairly uniform a fair approximation of the antenna temperature can be made by considering the city to be a point source at the city center. The effective power radiated would then be the area of the city times the power density, C from Fig. 16. The temperature is then calculated using Eq. (6).

If on the other hand the conditions above are not valid or if a more precise calculation is desired a quick calculation can still be obtained by partitioning the city into annular sectors that have a constant illumination factor, $D(\theta, \phi)$. Using Eq. (3) and the geometry of Fig. 17 we get for a sector

$$T_a = \frac{P_r}{kB} = \frac{\lambda^2 G C}{16\pi^2 k} \int_{\phi_1}^{\phi_2} \int_{\theta_1}^{\theta_2} \cot\theta \, d\theta \, d\phi$$

$$= \frac{\lambda^2}{16\pi^2} \, G C (\phi_2 - \phi_1) \ln \frac{\sin\theta_2}{\sin\theta_1} \qquad (11)$$

where $G = G_o \, D(\theta, \phi)$

= antenna gain over the sector $a \cdot b$

From Fig. 17 we have:

$$\phi_2 - \phi_1 = \frac{a}{r_o}$$

$$\sin\theta_2 = \frac{h}{\sqrt{(r_o - \frac{b}{2})^2 + h^2}}$$

$$\sin\theta_1 = \frac{h}{\sqrt{(r_o + \frac{b}{2})^2 + h^2}} \qquad (12)$$

$$T_a = \frac{\lambda^2 G C}{32\pi^2 k} \frac{a}{r_o} \ln \left\{ \frac{\left(1+\frac{b}{2r_o}\right)^2 + \left(\frac{h}{r_o}\right)^2}{\left(1-\frac{b}{2r_o}\right)^2 + \left(\frac{h}{r_o}\right)^2} \right\} \qquad (13)$$

The sum of the temperatures from all the sections of the city defined above will give a good approximation to Eq. (3). Equation (13) normalized to $\lambda^2 G C$ is plotted in Fig. 18 as a function of b/r_o when $a = b$. Since the area of the sector is $a \cdot b$ the independent variable is equivalent to the square root of the sector area divided by r_o.

A special limiting case occurs when flying over a city center with an antenna that provides uniform illumination downward. Letting $a = b = 2r_o$ we define a triangular sector of a circle with radius $2r_o$. There are π such sectors in 360^o. Therefore if the city is circular with radius $2r_o$ we get:

$$T_a = \frac{\lambda^2 G C}{16\pi k} \ln \left[1 + \left(\frac{2r_o}{h}\right)^2 \right] \qquad (14)$$

The use of Fig. 18 to obtain a first approximation to the temperature level expected is illustrated with the aid of data taken on the C-135 with the upward looking blade antenna flying by the southern edge of Miami. The radiometer data is shown in Fig. 19. The flight path of the aircraft was south easterly to a point south and slightly west of the city where a turn was executed to the east, passing south of the city of Miami and crossing the coastline where the antenna temperature drops below 300^oK. Using Figs. 16 and 18 we can compute the expected antenna temperature. A rough approximation of the Urban area is to assume it to be a sector with $a = b$ so that:

$$r_o = 12 \text{ mi.}$$

$$b = \sqrt{117} = 10.8 \text{ mi.}$$

$$h = 6.6 \text{ mi.}$$

$\therefore$ from Fig. 16

$$T = 300 \lambda^2 G_o C 10^{-18}$$

$$= 1475 G_o (^oK)$$

During the turn the antenna declination angle corresponding to the city center would be about 10^{o} which corresponds to an antenna gain of approximately + 1 db $\pm$ 1 db. The resultant expected additive temperature would be 1855^{o}K. As previously stated Miami appeared to exhibit temperature levels that differed by 3 db depending upon the time of year. Since Fig. 18 is based upon a "hot" Miami and the data of Fig. 19 was obtained in September we would expect a temperature one-half that calculated. In addition, the background noise temperature from the sky and earth of approximately 200^{o}K has to be added. The result is:

T expected	=	1128^{o}K $\pm$ 240^{o} "cold"
	=	2055^{o}K $\pm$ 480^{o} "hot"
T measured	=	1800^{o}K $\pm$ 180^{o}

The discrepancy between the actual and expected temperature can be attributed to the approximation of the city geometry, the fact that surrounding suburban areas are not considered in the calculation, and that the value of C_x for Miami varies by at least + 3 db as a function of the time of year.

After the turn was completed the aircraft flew south of the city in level flight with a resultant measured temperature of approximately 1300^{o}K. Assuming a -1 db $\pm$ 1 db antenna gain in the direction of the city we get

T expected	=	935^{o}K $\pm$ 190^{o} "cold"
	=	1670^{o}K $\pm$ 380^{o} "hot"
T measured	=	1300^{o}K $\pm$ 130^{o}

VI. CONCLUSIONS:

The noise level inherent to airborne UHF antenna systems has been measured and characterized. The contributors to the overall noise level have been identified and discussed with the exception of coherent RFI. The results are summarized as follows:

1. Galactic and Thermal Earth Radiation: These sources contribute a low level background noise level of $150^{\circ}K$ to $300^{\circ}K$ (low gain antenna). Measurements were in general agreement with estimated values.

2. P-Static: This source of noise is negligible if modern static dischargers are employed on the aircraft and care is taken in the antenna design.

3. Atmospherics: Noise levels measured due to lightning discharges were 6 to 10 db lower than expected based upon extrapolated data in the literature. However, burst levels of several thousand degrees Kelvin are common when within 10 to 20 miles of the discharge with peaks in the tens of thousands of degrees. Burst rates of 20/min. were measured with typical burst width of 1/4 second.

4. City Noise: Analysis of data taken over cities in the Eastern United States indicates that the city can be modeled electromagnetically as a distributed aperture of random sources with uniform power density. The power density was calculated to be 3×10^{-18} to 1×10^{-18} watts/m^2/Hz over the UHF band. This value of power density was common to all cities during the weekday with the exception of New York City which had a 5-6 db higher level. Relations have been derived and curves plotted to compute antenna temperature increase due to city noise based upon the metropolitan area and range.

APPENDIX A

Measurement Equipment

The equipment used on the C-135 and C-131 was the same with the exception of the antenna. A block diagram of the measurement equipment is shown in Fig. A-1.

An ARI calibrated variable noise source was used during the measurements for data calibration. The triplexer shown was fabricated from existing coaxial cavities and was tuned to center frequencies of 226.2 MHz, 305.5 MHz and 369.2 MHz. The 3 db bandwidth of the triplexer was 1.6 to 1.7 MHz with greater than 80 db rejection at $\pm$ 10 MHz from center frequency. Low noise (300°K) preamps were in each channel prior to the channel radiometer. The radiometers shown were total power radiometers with a 2 msec integration time and a 1.2 MHz bandwidth. The outputs of the radiometers were amplified and recorded on a 7 channel FM P.I. recorder. One of the 7 channels was used for voice commentary, the remaining 6 used to record high and low sensitivity signals from the 3 radiometers. A 2 channel T.I. chart recorder was used on board for monitoring purpose. Likewise a tunable wideband CEI receiver was used on the aircraft to monitor the three channels. Individual line spectra in the 1.2 MHz wide channels could be identified using the CEI built-in spectral display.

The antenna used on the C-131 was a 2 dipole array mounted over a flat ground plane, the combination mounted under the aircraft fuselage near the aircraft tail. The average E and H plane half power beamwidth's at the three operating frequencies were 42° and 112° respectively, the beam peak facing earthward. The antenna was matched at the three operating frequencies to a VSWR of less than 1.5:1.

A standard military blade antenna (AT-256) was used on the C-135. The antenna mounted on the top rear of the fuselage produced a donut-shaped pattern roughly symmetrical about the vertical. The radiation was primarily upward. An estimation of the percentage downward illumination was computed

using typical scaled-model pattern, produced by Boeing, of the antenna on a C-135. The fore-aft elevation pattern differs from the broadside elevation pattern due to the increased ground plane along the fuselage and the tail assembly. The percentage of illumination vs. elevation angle is shown in Fig. A-2, where the elevation pattern at broadside and fore-aft are considered separately and as figures of revolution about the vertical and:

$$K(\psi) = 2\pi G_o \int_0^{\psi} E^2(\psi) \sin \psi \, d\psi \qquad (A-1)$$

An estimate of the total downward illumination by the average $K(\psi)$ is shown in Fig. A-2.

APPENDIX B

Antenna Illumination

In order to estimate $C(\theta, \phi)$ several approximations are made. From all the data taken during this program, plus noise measurements made by others on the ground, the noise density does not vary greatly within an urban area or for that matter from city to city. $C(\theta, \phi)$ is therefore approximated by a constant within the beam illuminated portion of the city and Eq. (3) of the text can be written as:

$$T_a = \frac{\lambda^2}{16\pi^2 k} \; C G_o \int_{\phi_1}^{\phi_2} \int_{\theta_1}^{\theta_2} D(\theta, \phi) \cot \theta \, d\theta \, d\phi \qquad \text{(B-1)}$$

Where the limits of integration correspond to the city limits and $G_t(\theta)$ is assumed to be unity. C can be computed once the value of the integral in B-1 is solved. However, the evaluation of this integral involves obtaining complete contour radiation patterns and then use of a computer for the evaluation. This effort is not consistent with the accuracy of the knowledge of the airborne antenna radiation pattern or with the assumption of constant C. Fortunately, a good analytical approximation to the radiation pattern can be made and with some effort an analytical expression for the integral obtained.

The principal plane patterns of the test antenna have been measured. The magnitude of the radiation pattern between the principal planes falls in between these values forming an elliptically shaped beam. For cases where the ratio of the principal axes of the "ellipse" is not too large, i.e., for most of the main beam a reasonable and convenient expression for the main beam radiation pattern using the geometry of Fig. B-1 is:

$$D(\psi, \phi) = E_h^2(\psi) \cos^2\phi + E_e^2(\psi) \sin^2\phi \qquad \text{(B-2)}$$

where

$$\psi = \frac{\pi}{2} - \theta$$

$E_h^2(\psi)$ = normalized H-plane radiation pattern

$E_e^2(\psi)$ = normalized E-plane pattern

The measured principal plane patterns are shown in Figs. B-2 and B-3 along with simple functions that are good approximations to the E-plane and H-plane pattern at all three frequencies. The integral of Eq. (B-1) can now be written as:

$$I = 4\int_0^{\frac{\pi}{2}}\int_0^{\psi(\phi)} E_h^2(\psi) \cos^2\phi \tan\psi \, d\psi \, d\phi + 4\int_0^{\frac{\pi}{2}}\int_0^{\psi(\phi)} E_e^2(\psi) \sin^2\phi \tan\psi \, d\psi \, d\phi \qquad \text{(B-3)}$$

where

$$\begin{aligned}
E_h^2(\psi) &= \cos^2\psi && -\tfrac{\pi}{2} < \psi < \tfrac{\pi}{2} && f = 305.5 \text{ MHz and } 226 \text{ MHz} \\
&= 0 && \tfrac{\pi}{2} < |\psi| && \\
&= .975 && -\tfrac{\pi}{4} < \psi < \tfrac{\pi}{4} && f = 369.2 \text{ MHz} \qquad \text{(B-4)} \\
E_e^2(\psi) &= \cos^2 2\psi && -\tfrac{\pi}{4} < \psi < \tfrac{\pi}{4} && \\
&= 0 && \tfrac{\pi}{4} < |\psi| &&
\end{aligned}$$

The beam contours obtained from the approximate analytic expression at 305.5 MHz are plotted in Fig. B-4 along with the measured contour obtained from the principal plane and 45^{o} plane patterns.

The limits of integration are defined by Fig. B-5. The component of I due to $E_h^2(\psi)$ at 226.2 MHz and 305.5 MHz is:

$$I_h = 4 \int_0^{\frac{\pi}{2}} \int_0^{\tan^{-1} a} \sin\psi \cos\psi \cos^2\phi \, d\psi \, d\phi \qquad \text{(B-5)}$$

where

$$a = \frac{\tan\psi_o}{\cos\phi}$$

Performing the integration we get for $\psi_o < \frac{\pi}{2}$

$$I_h = \pi \tan^2 \psi_o (1 - \sin\psi_o) \qquad \text{(B-6)}$$

At 369.2 MHz the $E_h^2(\psi)$ contribution is:

$$I_h = 4 \int_0^{\frac{\pi}{2}} \int_0^{\tan^{-1} a} .975 \tan\psi_o \cos^2\phi \, d\psi \, d\phi \qquad \text{(B-7)}$$

which results in Eq. B-8 for $\psi_o < \frac{\pi}{4}$

$$I_h = .975\,\pi \left[\ln \frac{1 + \sin\psi_o}{\cos\psi_o} - \frac{\sin\psi_o}{1 + \sin\psi_o} \right] \qquad \text{(B-8)}$$

The E-plane contribution to the integral I is constant when $\psi_o < \frac{\pi}{4}$ since $E_e^2(\psi) = 0$ for $\psi > \frac{\pi}{4}$. This constant is equal to:

$$I_e = 4 \int_0^{\frac{\pi}{2}} \int_0^{\frac{\pi}{4}} \cos^2 2\psi \sin^2 \phi \tan \psi \, d\psi \, d\phi$$

$$= -\frac{\pi}{4} (4 \ln .707 + 1) = .301 \text{ for } \psi_o \geq \frac{\pi}{4} \qquad \text{(B-9)}$$

When ψ_o is less than $\frac{\pi}{4}$ the integral I_e is the sum of two integrals defined by the limits derived from Fig. B-5. These limits are:

Sector I — ψ varies from 0 to $\tan^{-1} \frac{\tan \psi_o}{\cos \phi}$

ϕ varies from 0 to $\cos^{-1} (\tan \psi_o)$

Sector II — ψ varies from 0 to $\frac{\pi}{4}$

ϕ varies from $\cos^{-1} (\tan \psi_o)$ to $\frac{\pi}{2}$ (B-10)

The integral over the Sector II limits is relatively straightforward with the result:

$$I_{e_{II}} = .384 \left[\frac{\pi}{4} - \frac{\cos^{-1} \delta}{2} + \frac{\delta}{2} (1 - \delta^2)^{1/2} \right] \qquad \text{(B-12)}$$

where δ has been substituted for $\tan \psi_o$. Over Sector I the evaluation of the I_e results in*

*The integrals solved above are not simple due to the complexity of the limits. The solutions were obtained with the aid of integral tables in references 13 and 14.

$$I_{e_I} = \delta(1-\delta^2)^{1/2} - \frac{2\delta}{(1+\delta^2)^{1/2}} \tan^{-1}\left(\frac{1-\delta^2}{1+\delta^2}\right)^{1/2} - 2\delta\cos^{-1}\delta$$

$$+ 2\delta(1-\delta^2)^{1/2}\left[.96 + .12\delta^2 + .108\delta^4 + .091\delta^6\right] \qquad \text{(B-13)}$$

where the last term of B-12 was obtained from the integration of the first four terms of series expansion of $\ln\left(1 + \frac{\delta^2}{\cos^2\phi}\right)$.

In summary the value of I at the two lower frequencies:

$$I = \pi\tan^2\psi_o\,(1-\sin\psi_o) + I_{e_I} + I_{e_{II}} \qquad \psi_o < \frac{\pi}{4}$$

$$= \pi\tan^2\psi_o\,(1-\sin\psi_o) + .301 \qquad \frac{\pi}{4} < \psi_o < \frac{\pi}{2} \qquad \text{(B-14)}$$

at 369.2 MHz for $\psi_o < \frac{\pi}{4}$ we get:

$$I = .975\pi\left[\ln\frac{1+\sin\psi_o}{\cos\psi_o} - \frac{\sin\psi_o}{1+\sin\psi_o}\right] + I_{e_1} + I_{e_2} \qquad \text{(B-15)}$$

The value of I was not evaluated at 369.2 MHz for $\psi_o < \frac{\pi}{4}$ since the straight line approximation for E_n^2 results in an integral that is not solvable in closed form plus the fact that most of the experimental data obtained and analyzed corresponds to $\psi_o < \frac{\pi}{4}$.

I (ψ) is shown plotted in Fig. 11 of the text.

ACKNOWLEDGMENT

The author is indebted to D. Karp, R. V. Locke, and W. C. Provencher for their advice and efforts in the design and fabrication of the measurement equipment. The many flight hours logged by the above and S. B. Russell in accumulating the test data is also gratefully acknowledged.

REFERENCES

1. "Ground Terminal Noise Minimization Study - Final Report," No. WDL-TR 1972, Philco (18 January 1963), Contract No. AF 04 (695) -113, Sec. 2,3.

2. H. C. Ko, "The Distribution of Cosmic Radio Background Radiation," Proc. IRE, 46, 208 (Jan. 1958).

3. D. C. Hogg and W. W. Mumford, "The Effective Noise Temperature of the Sky," The Microwave Journal p. 80 (March 1960).

4. S. N. C. Chen and W. H. Peake, "Apparent Temperatures of Smooth and Rough Terrain," IRE Transactions on Antennas and Propagation, p. 567 (Nov. 1961).

5. Handbook of Geophysics (The MacMillan Co., New York, 1960), p. 9-1.

6. Advances in Radio Research, 2, 121 (Academic Press, London, New York, 1964).

7. R. L. Tanner and J. E. Nanevicz, "An Analysis of Corona-Generated Interference in Aircraft," Proc. IEEE, 52, 44 (Jan. 1964).

8. J. E. Nanevicz and R. L. Tanner, "Some Techniques for the Elimination of Corona Discharge Noise in Aircraft Antennas," Proc. IEEE, 52, 53 (Jan. 1964).

9. "UHF Aircraft Satellite Relay Final Report of Flight Tests," (Bendix Radio Div., Baltimore, Md., April 1965).

10. E. N. Skomal, "Distribution and Frequency Dependence of Unintentionally Generated Man-Made VHF/UHF Noise in Metropolitan Areas, IEEE Trans. on Electromagnetic Compatibility, Vol. EMC-7, 263 (Sept. 1965).

11. "Man-Made Noise" - Report to Technical Committee of the Advisory Committee for Land Mobile Radio Services from Working Group 3. (June 30, 1966).

12. "Reference Data for Radio Engineers," 4th Edition (ITT, New York, 1964) p. 763.

13. H. B. Dwight, "Tables of Integrals and Other Mathematical Data, 4th Edition (MacMillan Co., New York, 1961).

14. I. S. Gradshteyn and I. M. Ryzhik, "Tables of Integrals Series and Products," Academic Press (1965).

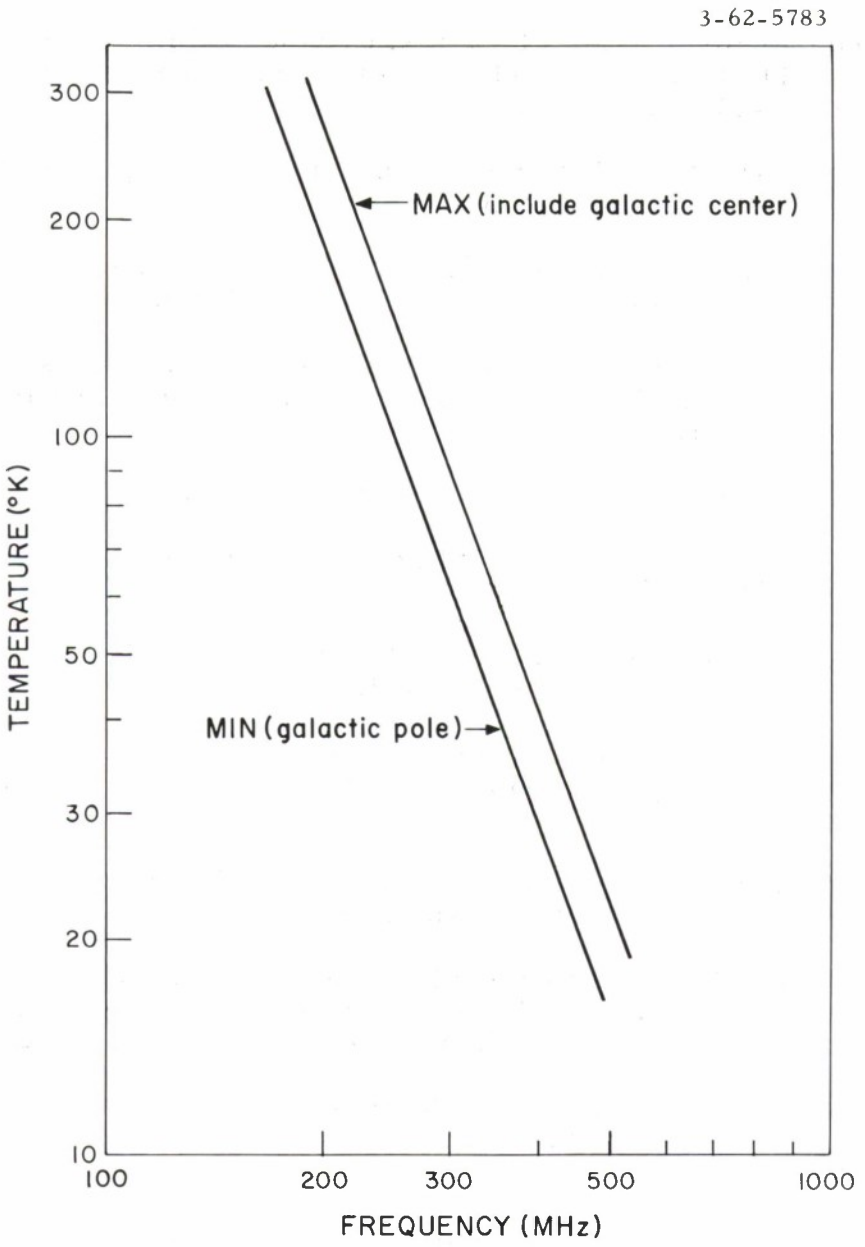

Fig. 1. Galactic temperature over a hemisphere.

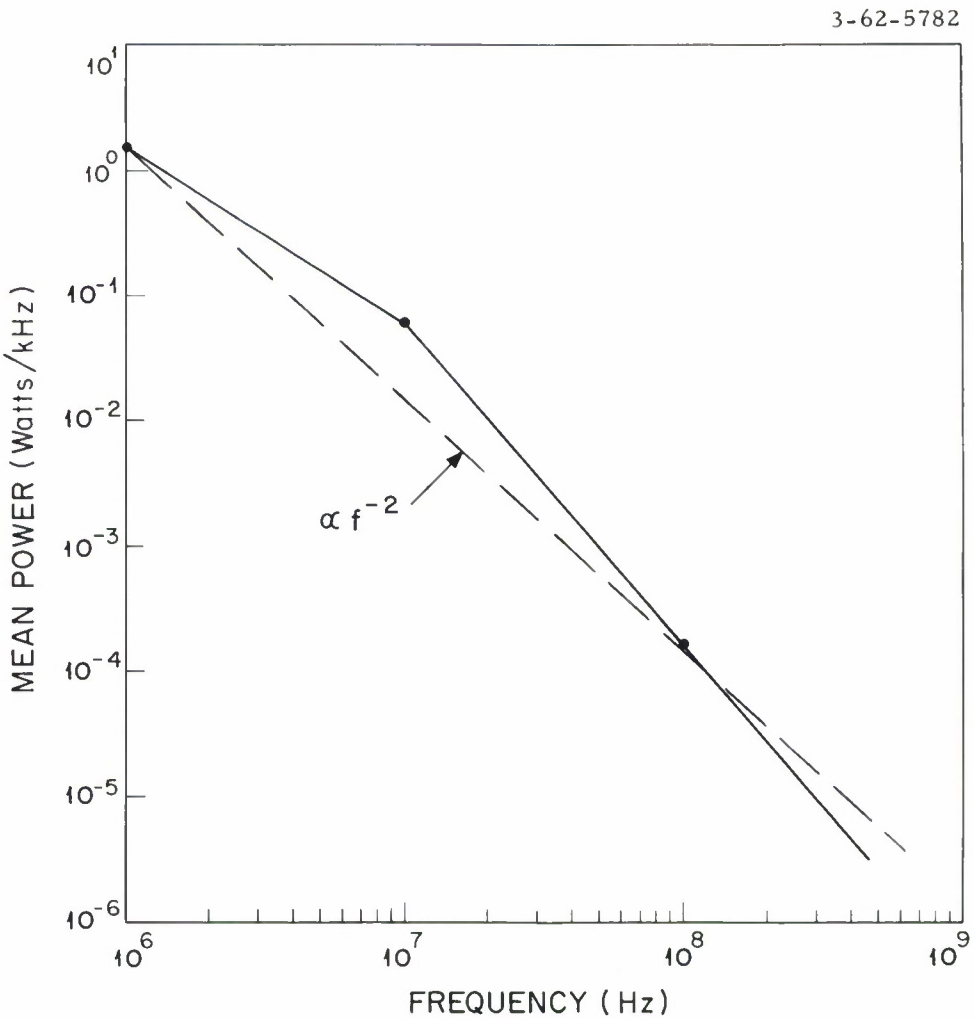

Fig. 2. Mean ERP of atmospheric disturbance.

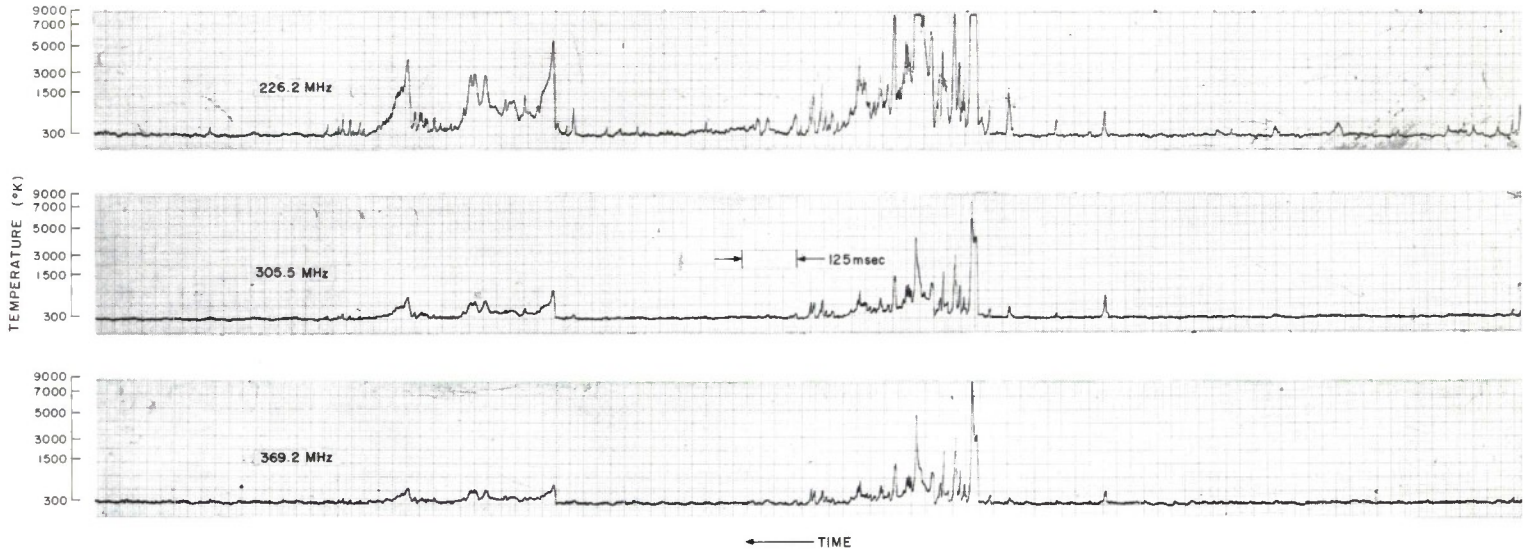

Fig. 3. Typical measured atmospheric disturbance.

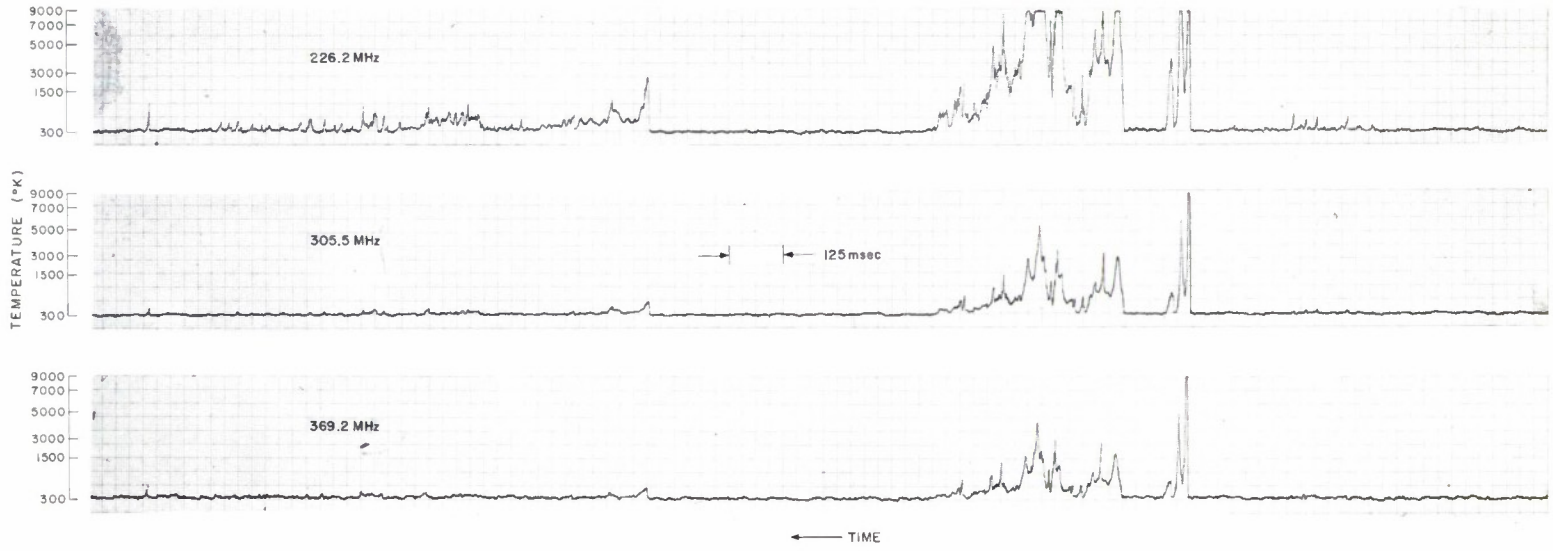

Fig. 4. Typical measured atmospheric disturbance.

-62-5776

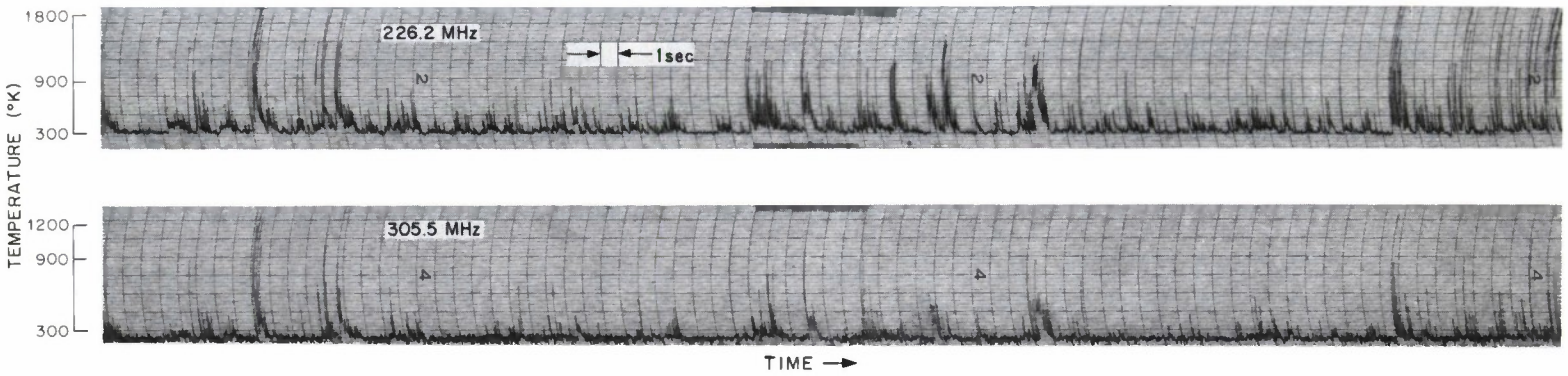

Fig. 5. Radiometer response near lightning storm.

-62-5828

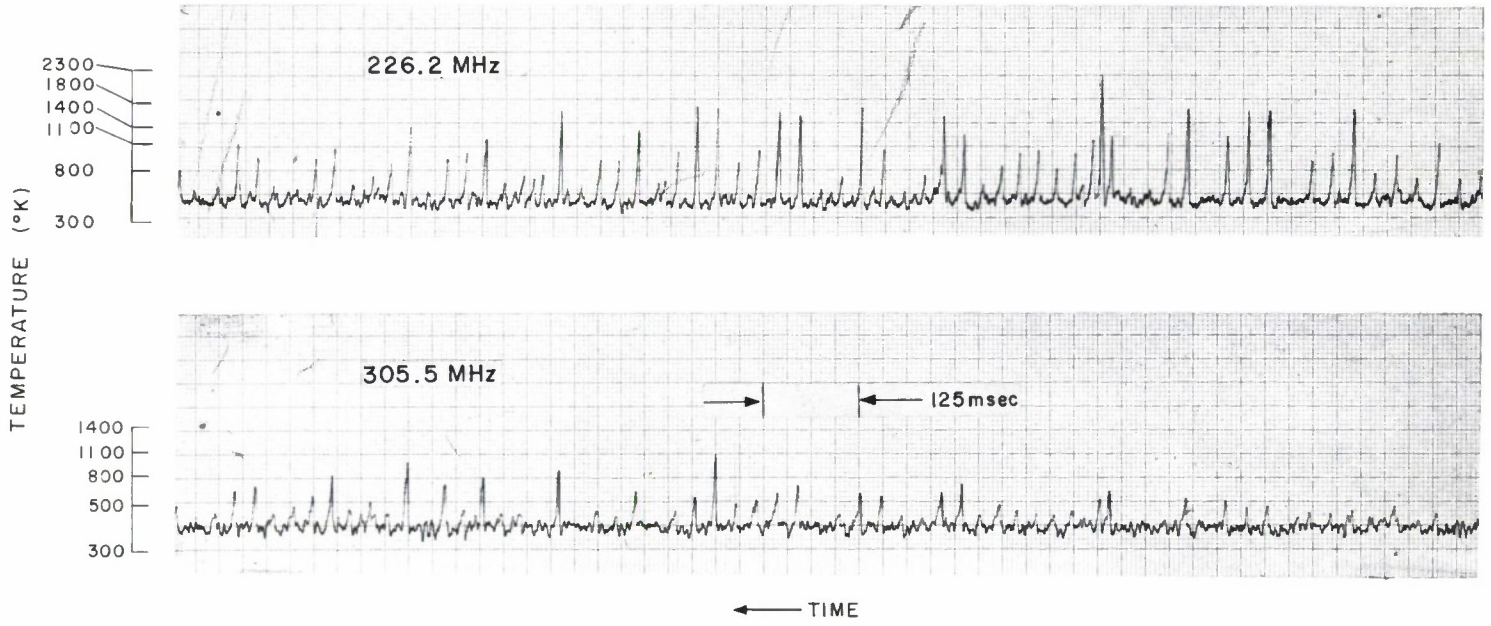

Fig. 6. Measured P-Static on C-131.

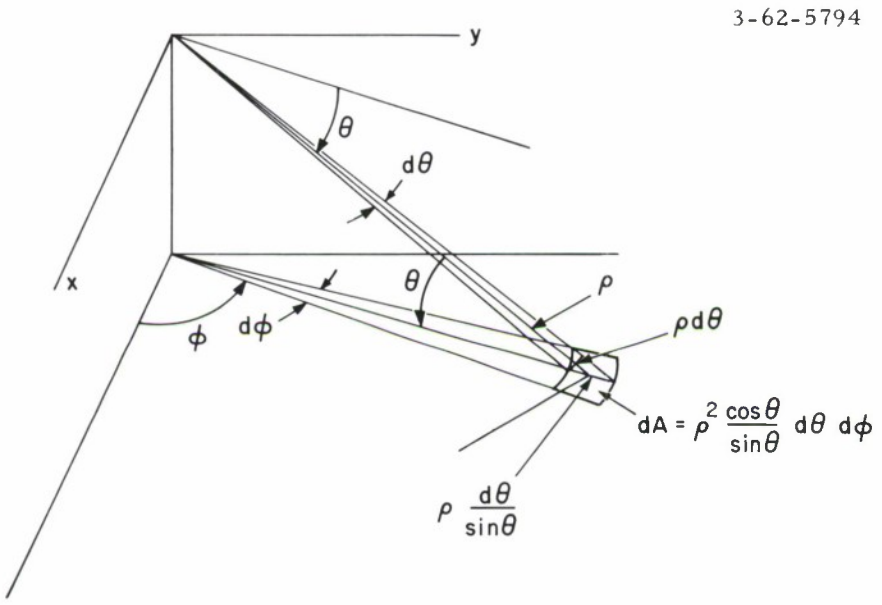

Fig. 7. Antenna coordinate system.

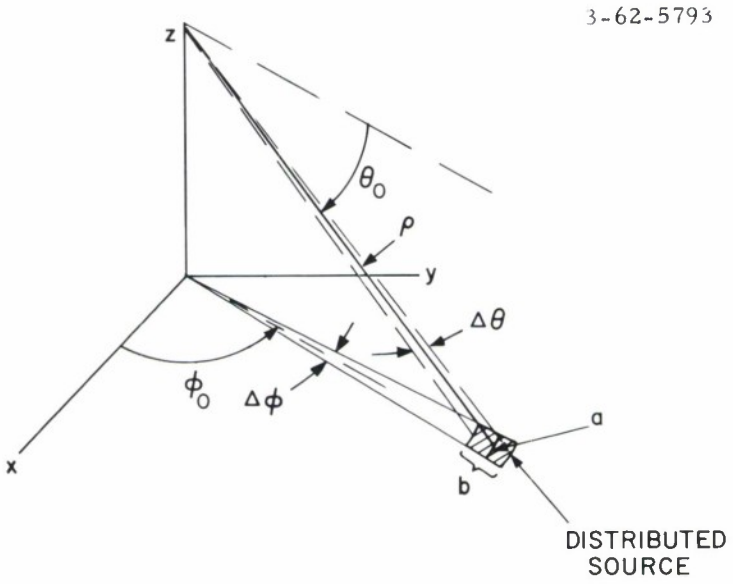

Fig. 8. Geometry when distributed source is small compared to range.

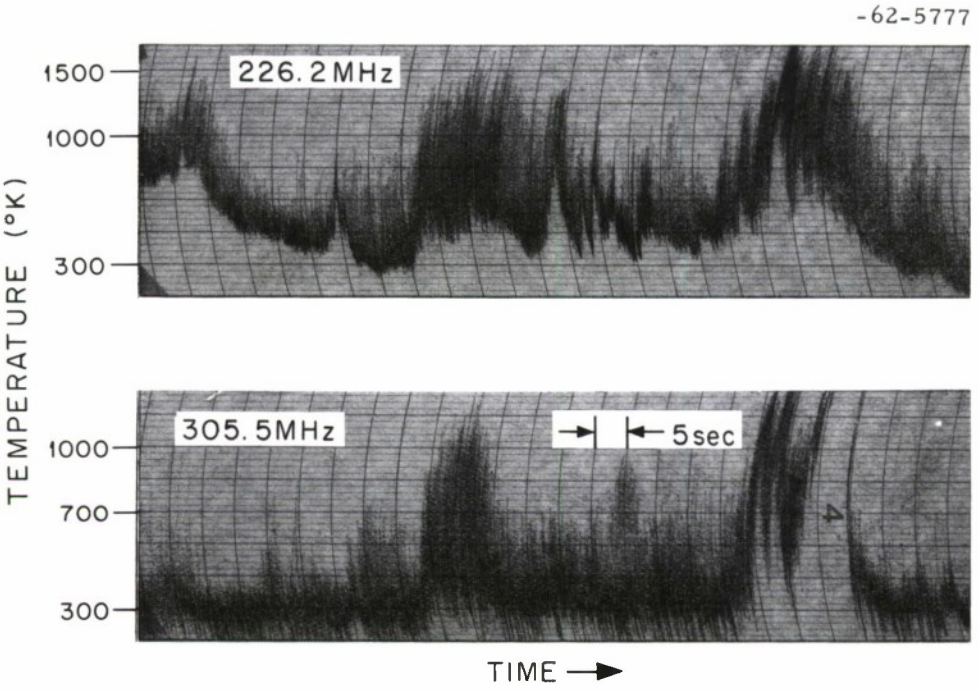

Fig. 9. Radiometer response over Rte. 128 at 2,000 ft.

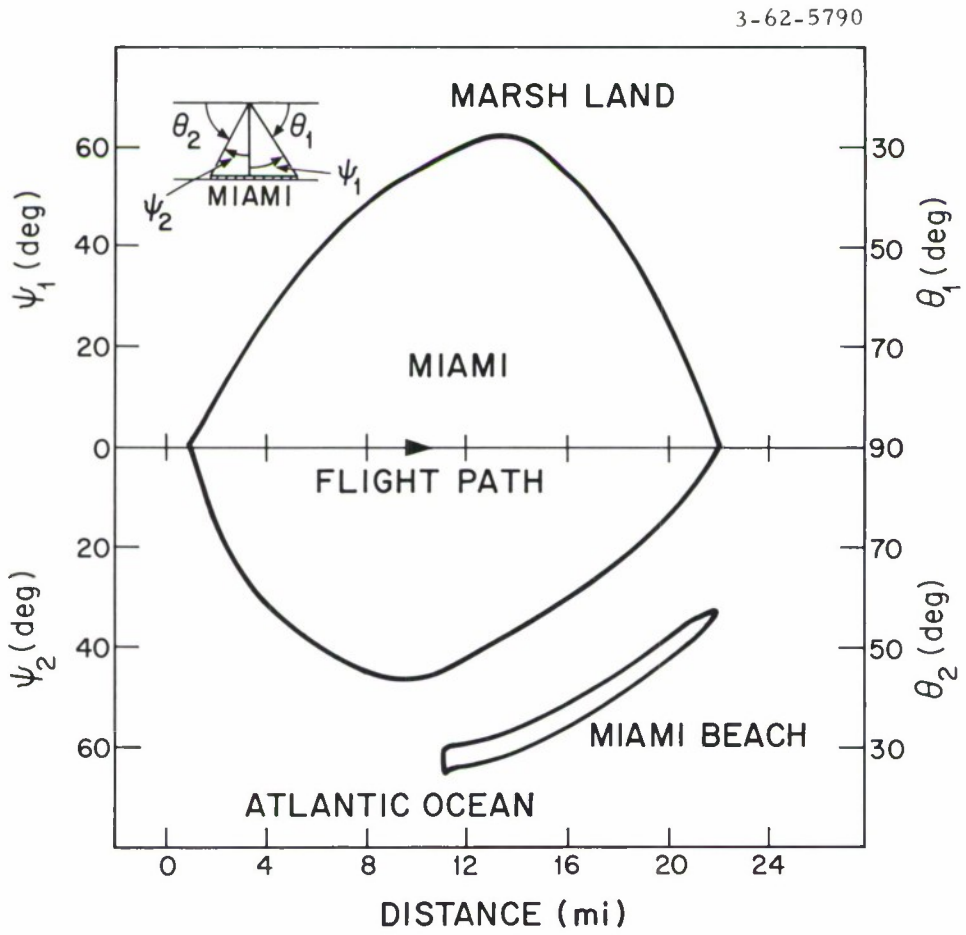

Fig. 10. Angular boundary of Miami at 18,000 ft.

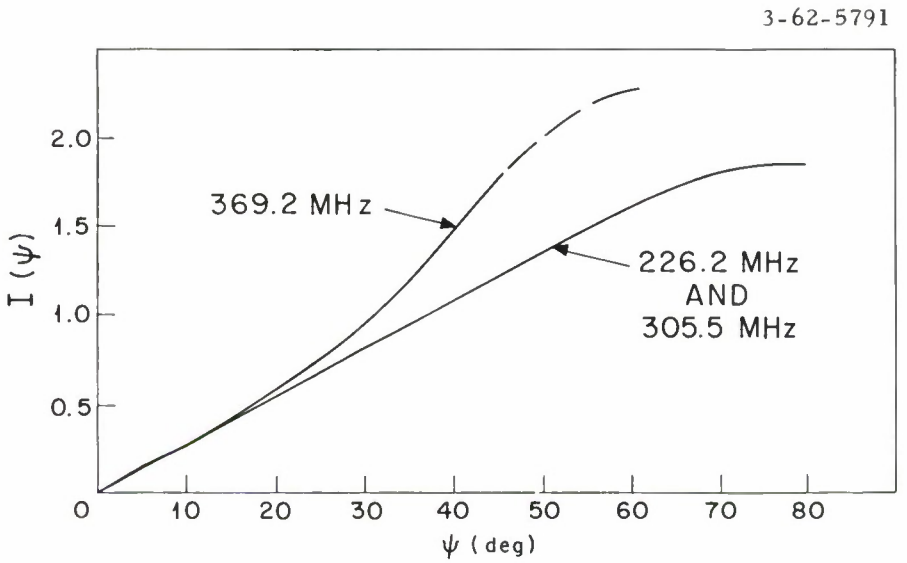
3-62-5791
2.0
1.5
1.0
0.5
I (ψ)
369.2 MHz
226.2 MHz
AND
305.5 MHz
0
10
20
30
40
50
60
70
80
ψ (deg)

Fig. 11. $I(\psi)$.

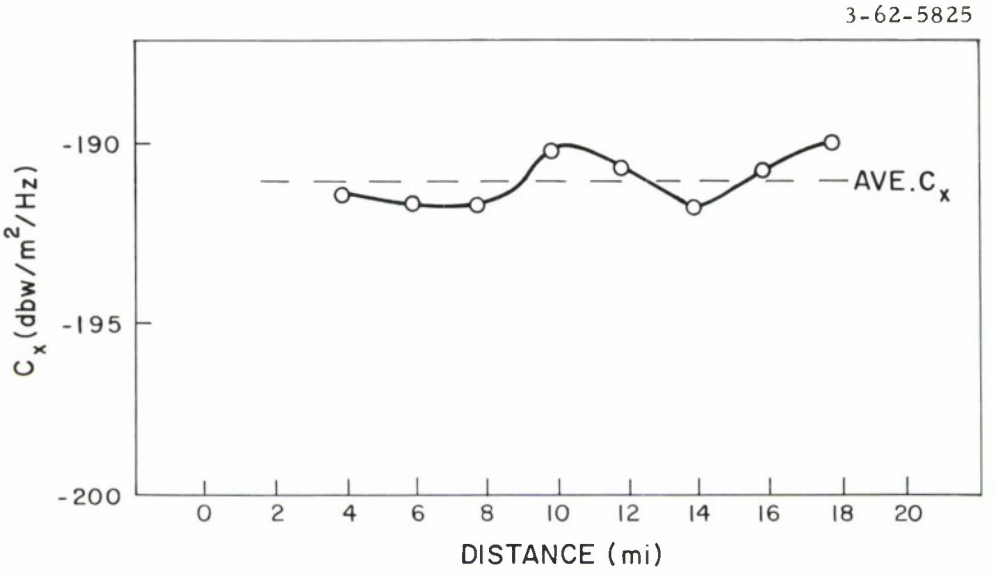

Fig. 12. Power density profile of Miami @305.5 MHz, 17 Nov. 1965.

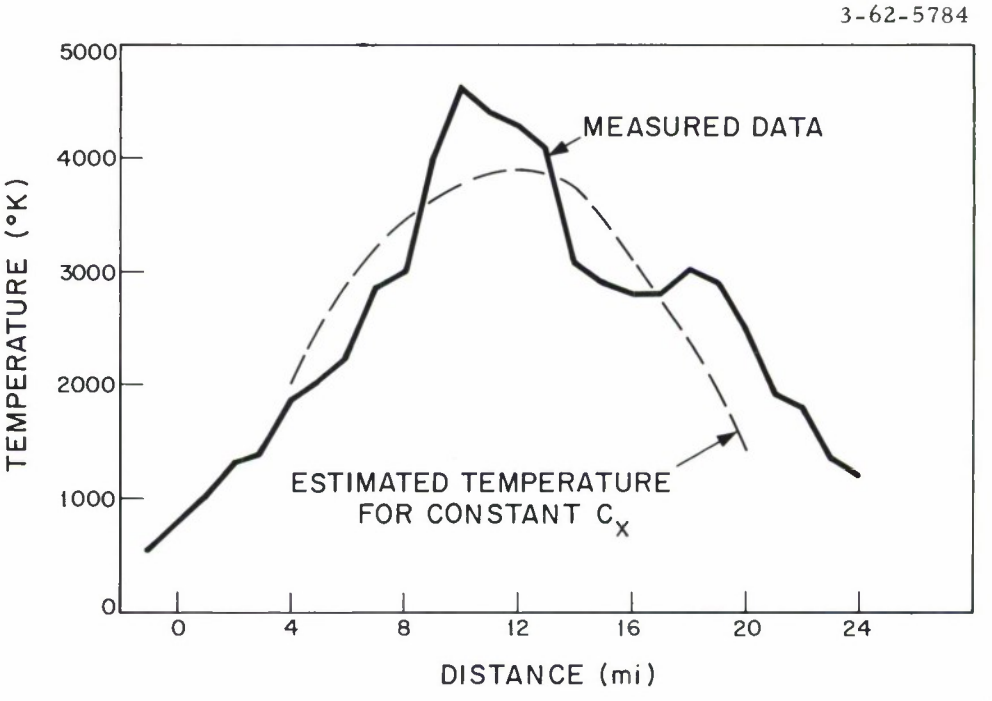

Fig. 13. Temperature profile of Miami @305.5 MHz, measured traveling North over city at 18K ft.

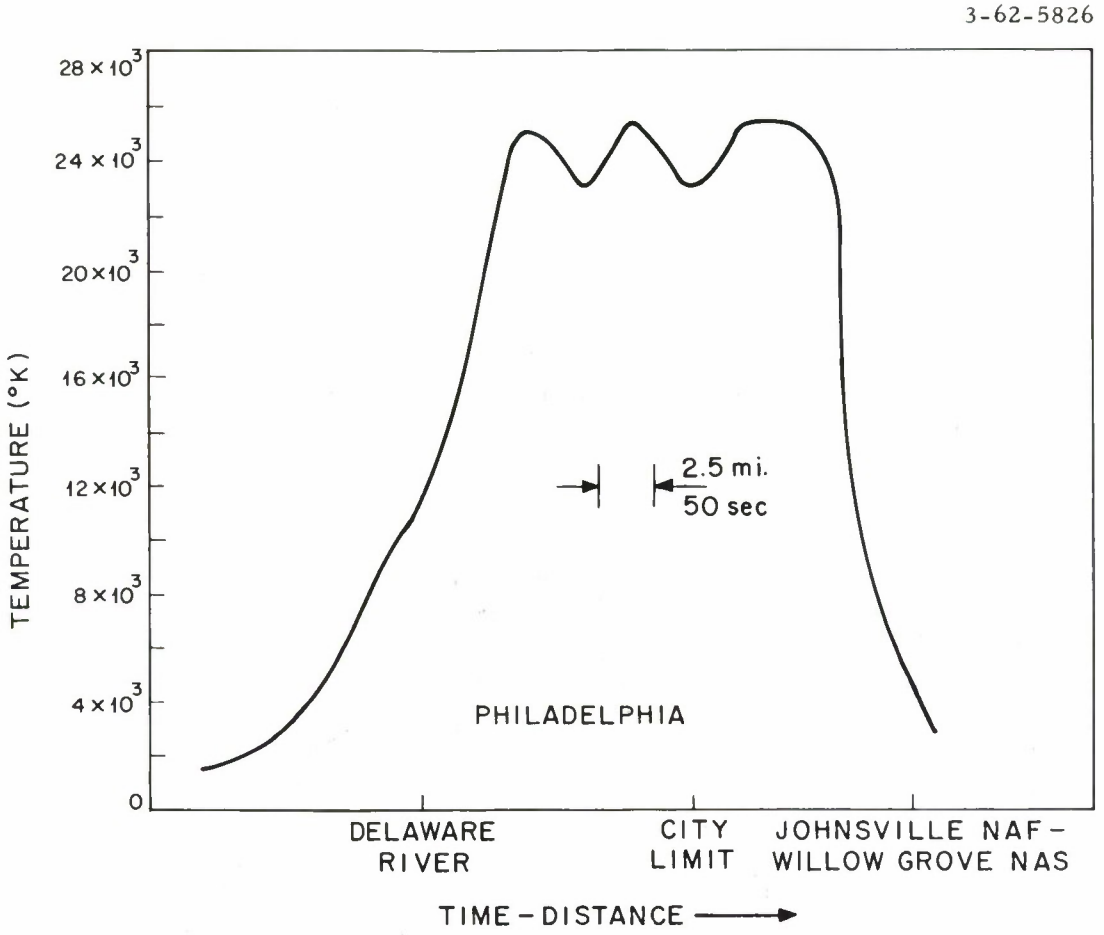

Fig. 14. Temperature profile of Philadelphia at 226.2 MHz, measured traveling North at 18K ft., 18 Nov. 1965.

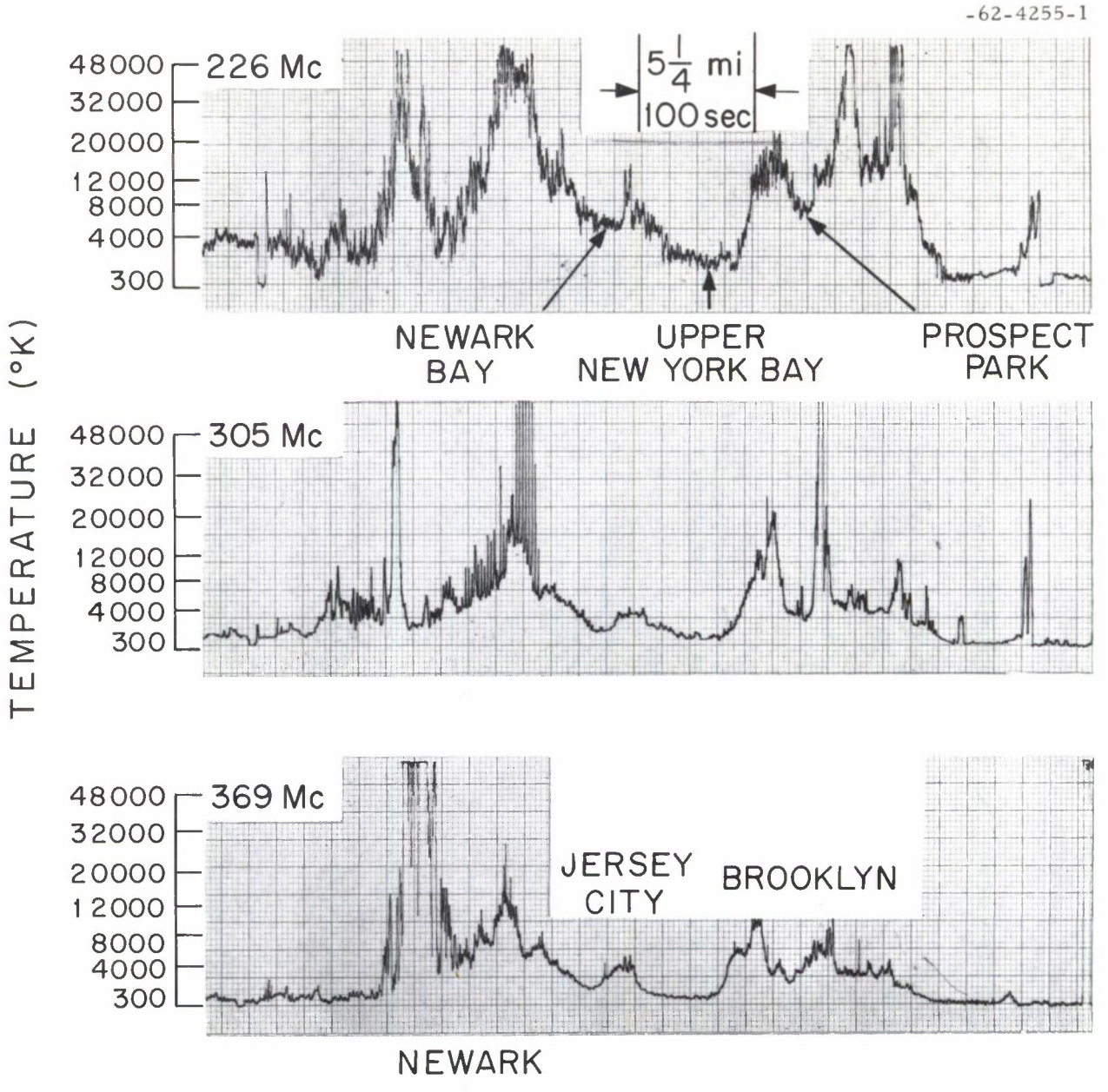

NOISE TEMPERATURE OF BROOKLYN-NEWARK AT UHF

MEASURED AT 2kft ALTITUDE AT 1400 EST, 18 NOV 1965

Fig. 15. Noise temperature over Brooklyn-Newark at 2K ft., 18 Nov. 1965.

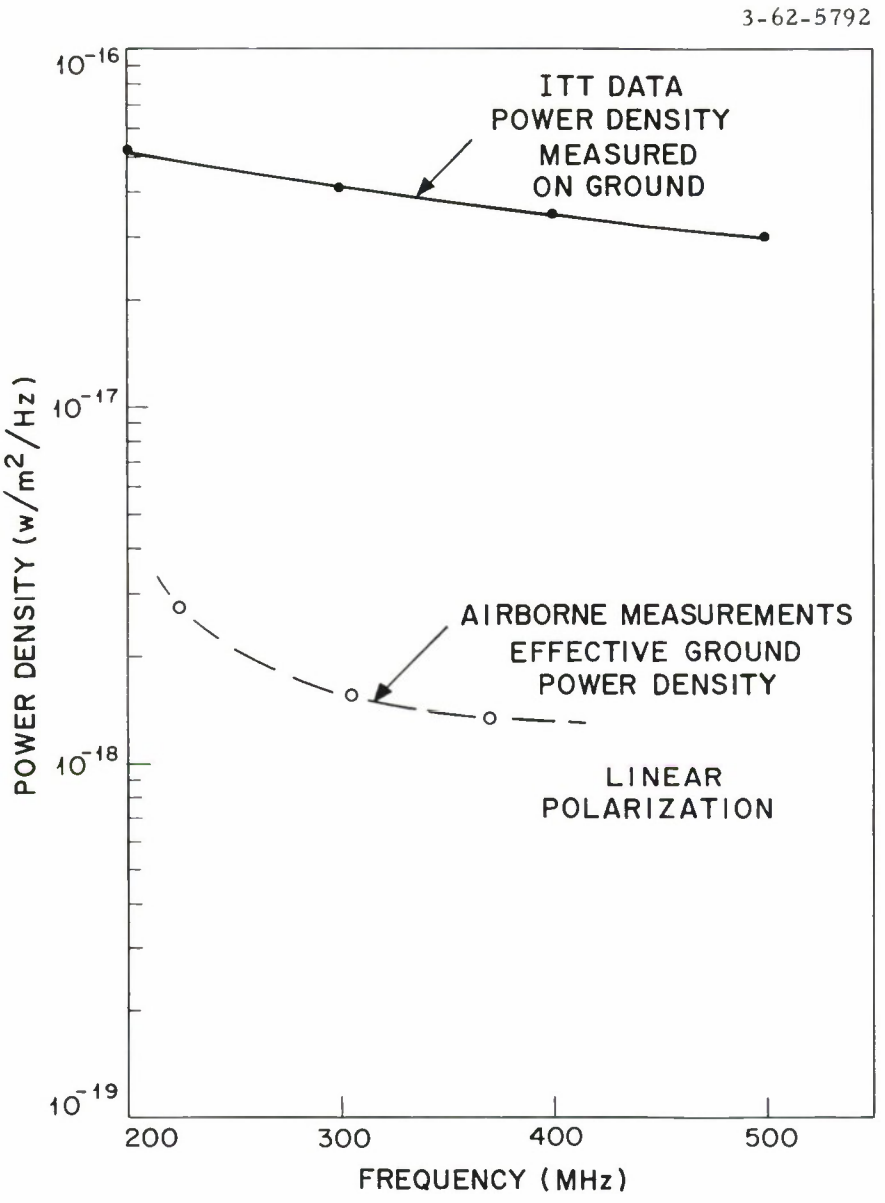

Fig. 16. Effective city power density.

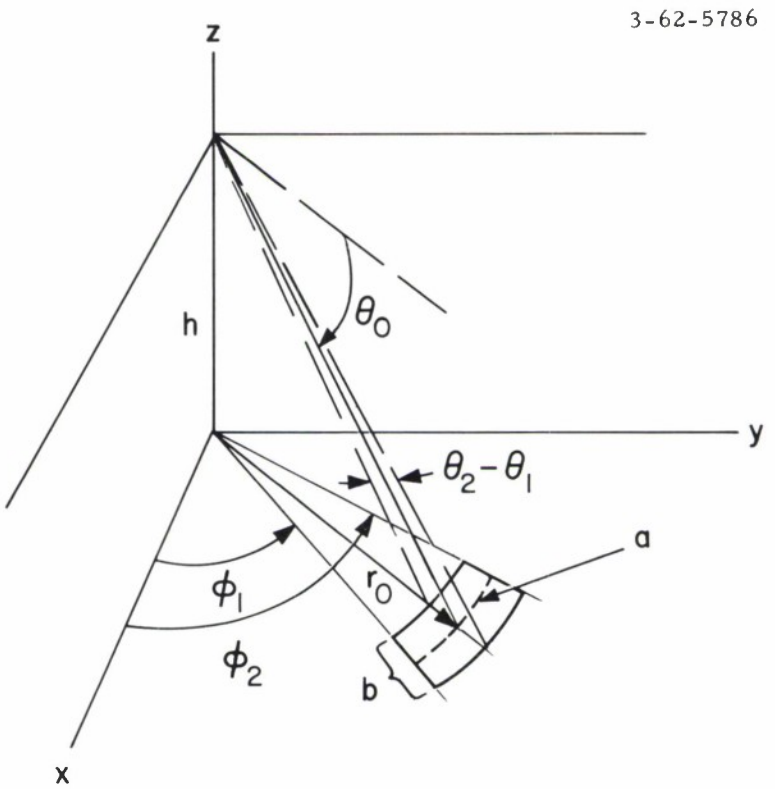

Fig. 17. Sector geometry.

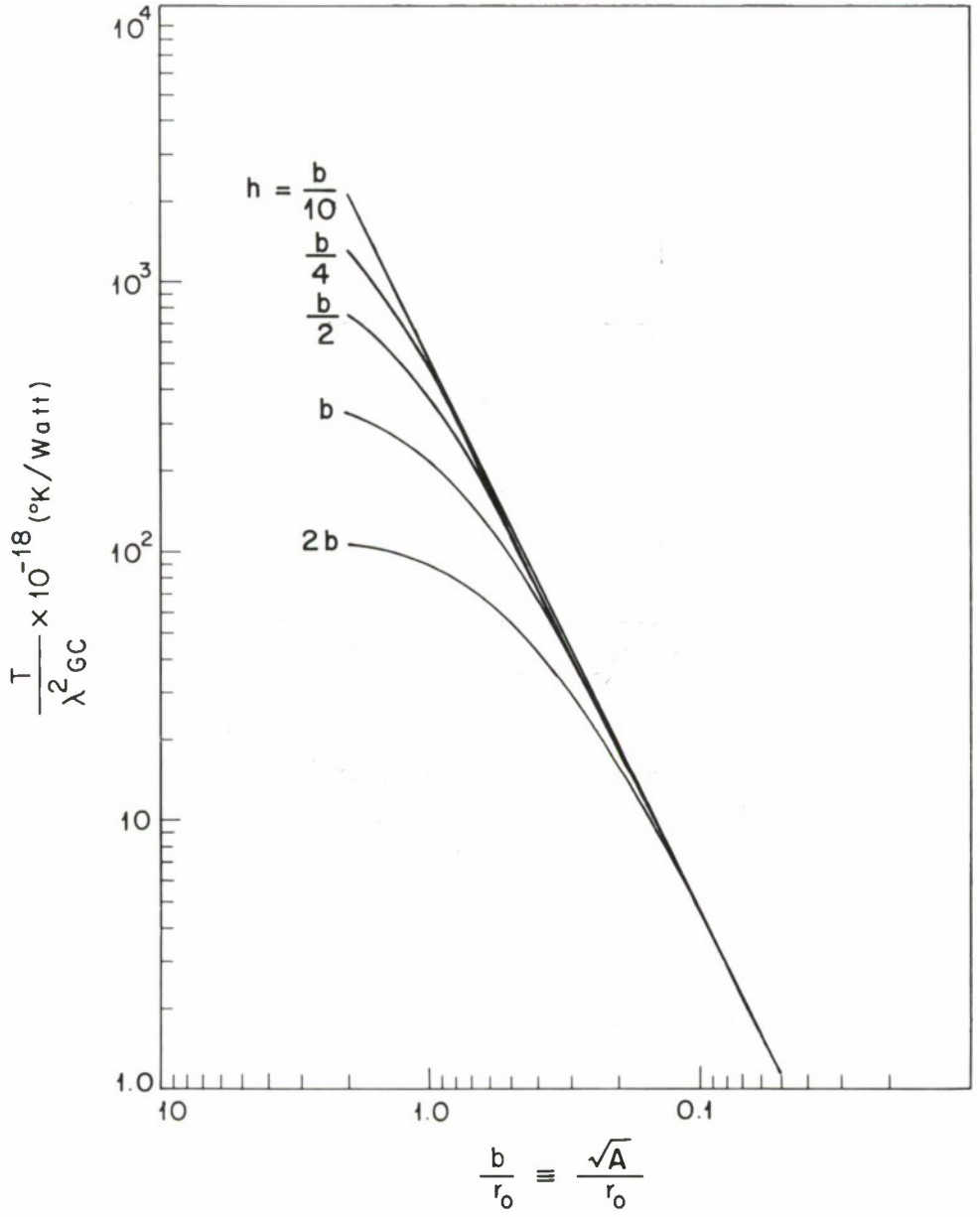

Fig. 18. Antenna temperature vs. area illuminated.

3-62-5381-1

HEADING SE TURNING 12 mi S OF MIAMI TO AN EASTERLY-HEADING MEASURED ON C-135 AT 35 kft ALTITUDE 14 SEP 1965

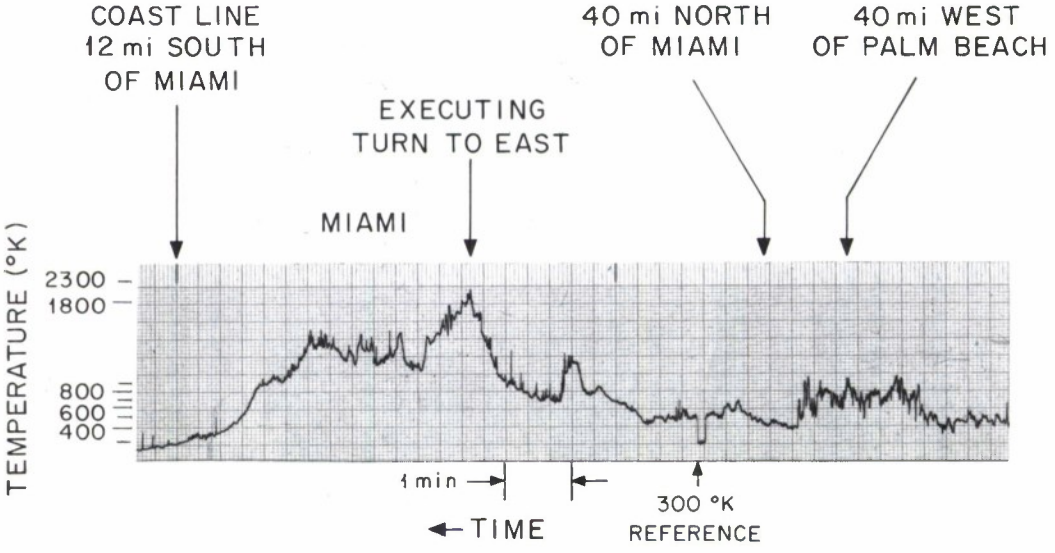

Fig. 19. Blade antenna temperature on C-135 at 226.2 MHz, measured near Miami at 35K ft., 14 Sept. 1965.

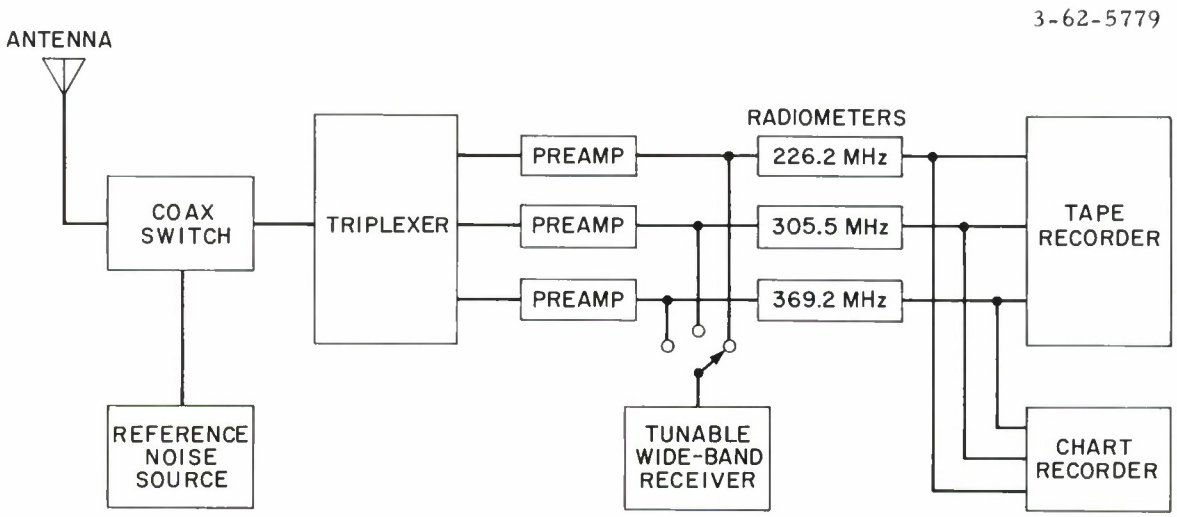

Fig. A-1. Measurement equipment.

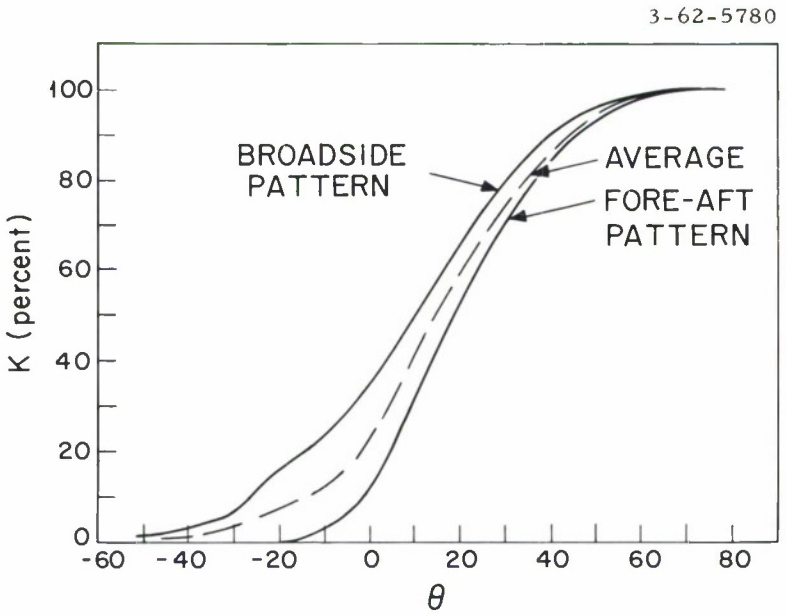

Fig. A-2. AT-256 illumination factor vs. elevation angle.

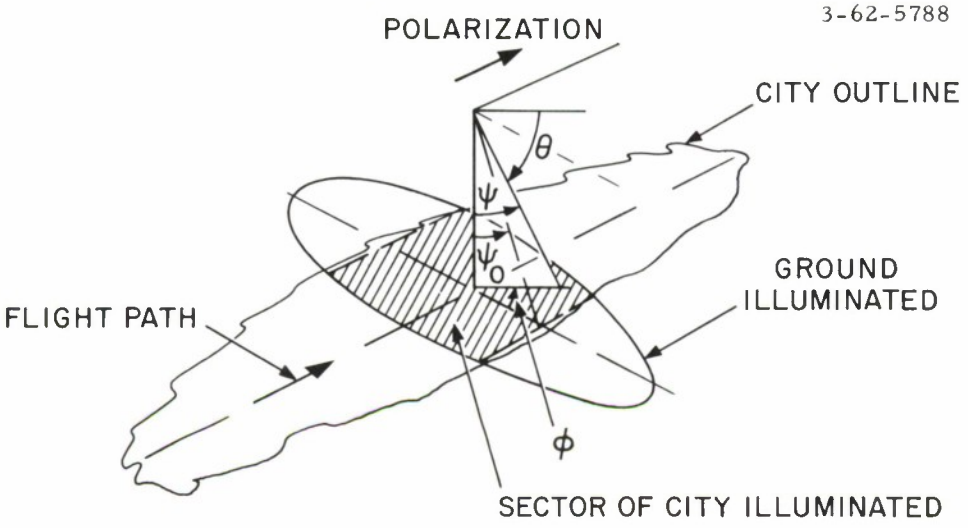

Fig. B-1. Mapping Geometry.

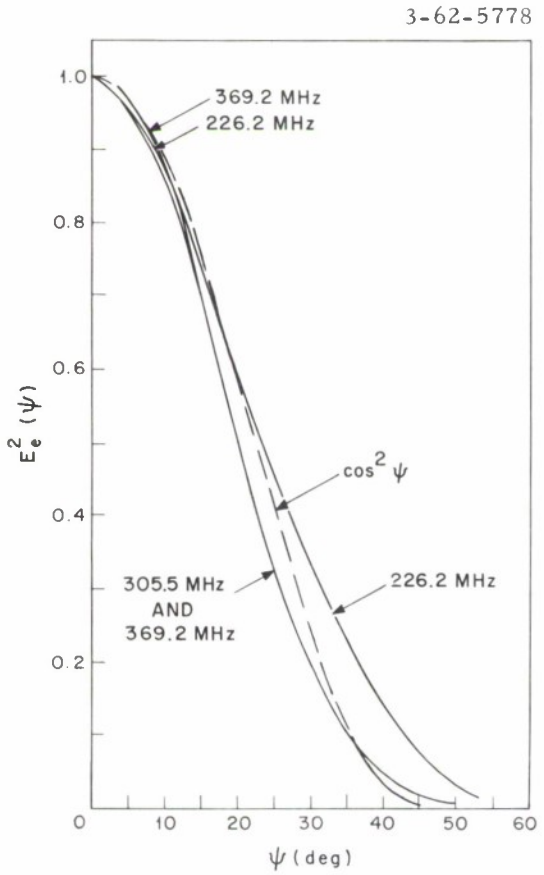

Fig. B-2. Antenna E-plane patterns.

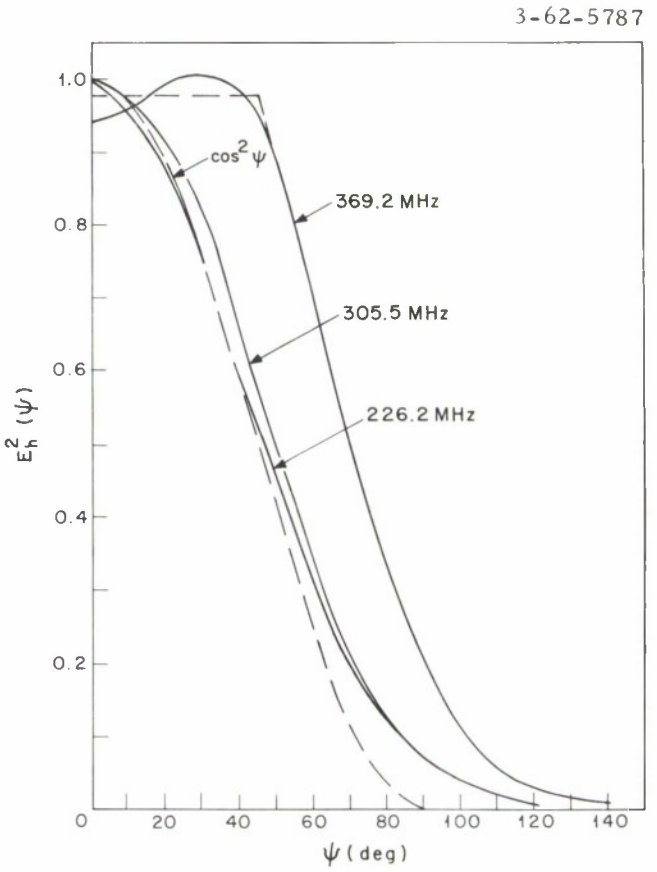

Fig. B-3. Antenna H-plane patterns.

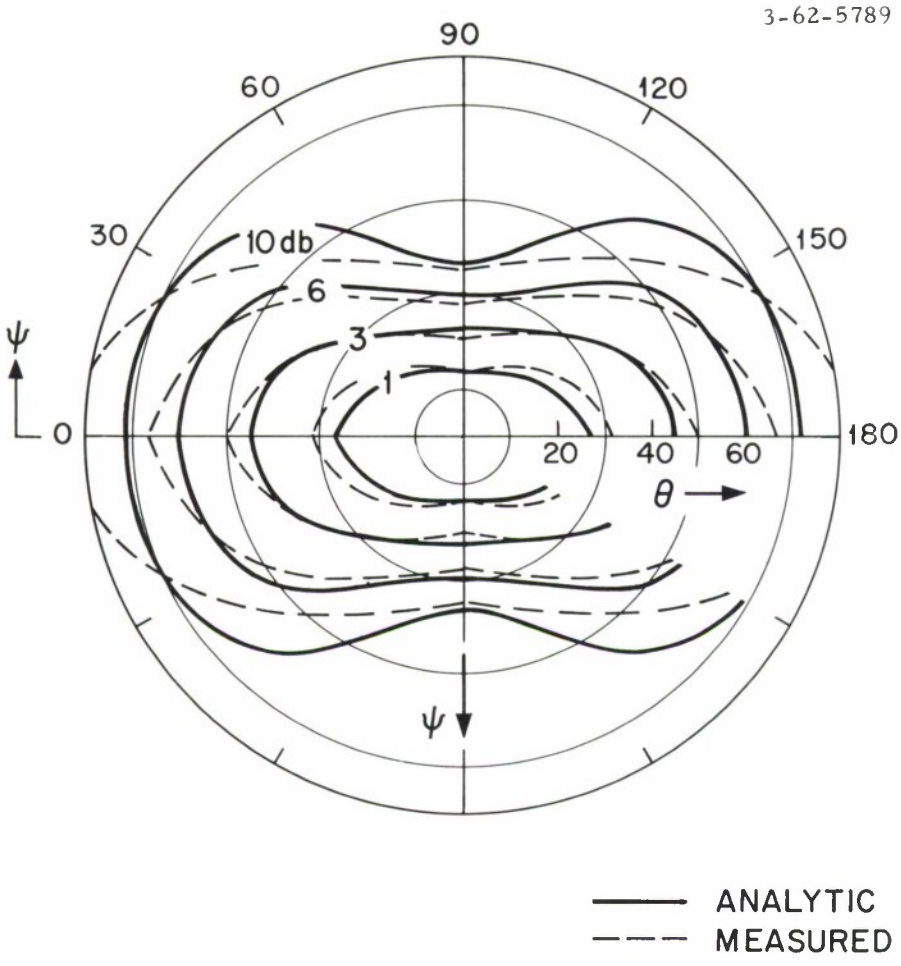

Fig. B-4. Contour plot of antenna pattern at 305.5 MHz.

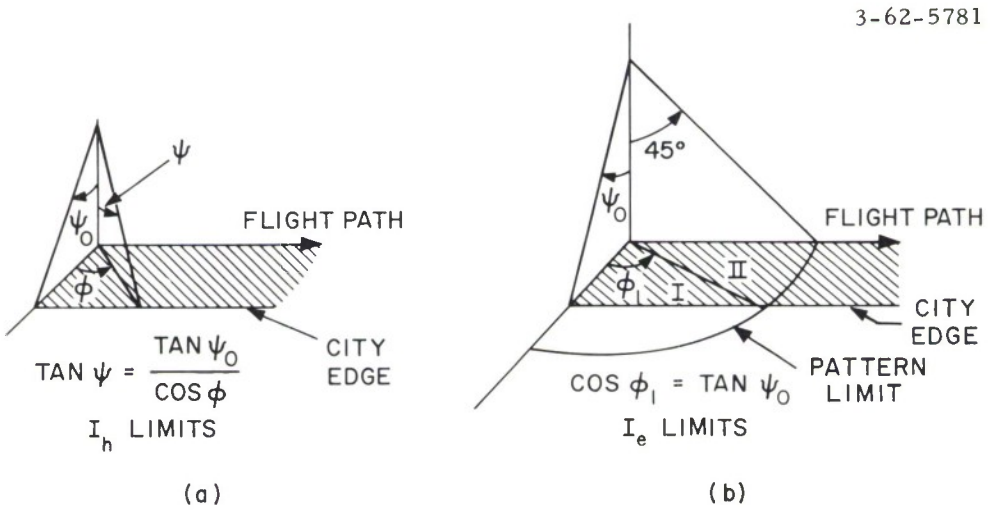

Fig. B-5. Limits of integration

DISTRIBUTION LIST

Director's Office

C. Robert Wieser
Gerald P. Dinneen
R. Joyce Harman

Archives

Division 3

S. H. Dodd
J. H. Chisholm
J. Ruze

Division 4

J. Freedman

Division 6

W. E. Morrow
P. Rosen

Group 61

L. J. Ricardi
B. F. LaPage
C. A. Lindberg

Group 62

I. L. Lebow
P. R. Drouilhet
K. L. Jordan
B. E. Nichols

R. Alter
J. H. Atchison
S. L. Bernstein
G. Blustein
Y. Cho
J. W. Craig
W. R. Crowther
J. D. Drinan
H. E. Frachtman
B. Gold
L. M. Goodman
D. H. Hamilton
H. H. Hoover
A. H. Huntoon
B. H. Hutchinson
D. Karp
R. V. Locke
A. A. Mathiasen
P. G. McHugh
N. J. Morrisson
F. Nagy
C. W. Niessen
G. Ploussios (6)
F. G. Popp
C. M. Rader
C. A. Reveal
S. B. Russell
T. S. Seay
I. Stiglitz
P. Stylos
J. Tierney
D. K. Willim

E. J. Aho
M. Alizeo
W. D. Chapman
P. Conrad
E. Cross
A. F. Dockrey
C. M. Foundyller
M. R. Goldberg
T. E. Gunnison
D. M. Hafford
L. F. Hallowell
J. M. Hart
D. A. Hunt
L. R. Isenberg
M. Kraatz
A. Lundin
J. V. Moscillo
W. C. Provencher
R. J. Saliga
T. Sarantos
J. F. Siemasko
R. S. Tringale
D. C. Walden
Group 62 Files

R. L. Bernier
J. T. Butterworth
J. V. Delsie
R. E. Drapeau
J. J. Drobot
E. W. Edman
P. R. Gendron
A. J. Grennell
A. V. Kesselhuth
R. M. Kokoska
A. L. Lipofsky
M. D. MacAskill
R. W. MacKnight
L. F. Mullaney
P. F. Murray
A. W. Olson
A. W. Pearson
J. R. Ritchie
S. Sawicki
C. H. Symonds
N. C. Vlahakis

Group 63

H. Sherman
D. C. MacLellan
P. Waldron
M. Ash
G. H. Ashley
R. S. Berg
A. Braga-Illa
C. Burrowes
R. W. Chick
N. B. Childs
J. B. Connolly
M. C. Crocker
A. I. Grayzel
B. Howland
C. L. Mack
J. Max
J. D. McCarron
R. E. McMahon
L. D. Michelove
B. J. Moriarty
D. M. Nathanson
D. Parker
J. L. Ryan
F. W. Sarles
W. G. Schmidt
V. J. Sferrino
I. I. Shapiro
R. L. Sicotte
W. B. Smith
D. M. Snider
A. G. Stanley
D. Tang
L. J. Travis
N. R. Trudeau
E. A. Vrablik

Group 64

P. E. Green
H. W. Briscoe
J. Capon
L. T. Fleck
P. L. Fleck
E. Gehrels
R. J. Greenfield
E. J. Kelly
R. J. Kolker
R. T. Lacoss
C. A. Wagner

Group 65

R. V. Wood
R. G. Enticknap
J. R. Brown
J. P. Densler
E. P. Edelson
R. A. Guillette
J. H. Helfrich
I. Wigdor

Group 66

B. Reiffen
J. U. Beusch
T. J. Goblick
B. E. White
H. L. Yudkin

Aerospace Corp.
2350 E. El Segundo Blvd.
El Segundo, Calif.

Arrowsmith, E. B.

Aerospace Corporation
San Bernardino Operations
San Bernardino, California 92402

Skomal, E. S.

Airborne Instruments Laboratory
Deer Park
Long Island, New York 11729

Aylward, William R., Jr.
Sielman, Peter F.

Air Force Avionics Laboratory
AVWC
Wright-Patterson Air Force Base,
Ohio, 45433

Boeing, Paul A.

Autonetics
Division of North American Aviation, Inc.
3370 Miraloma Ave.
Anaheim, Calif. 92803

Daniels, Robert L.
Jaffe, Richard M.
Reimherr, Robert N.

Avco Corp.
Electronics Division
Wilmington, Massachusetts 01887

Penndorf, Rudolf B.

Bendix Corporation
Bendix Radio Division
Baltimore, Maryland 21204

Betsill, Harry E.
Guntner, Urban A.
McComas, Arthur D.

Boeing Company
P.O. Box 3707
Seattle, Washington 98124

Dalby, Thomas G.
Freeman, Theodore K.
Galloway, William C.
Perkins, Leroy C.
Streets, Rubert B., Jr.

Boeing Company
Airplane Division
P.O. Box 707
Renton, Washington 98055

Axe, David C.

Booz-Allen Applied Research, Inc.
4733 Bethesda Ave.
Bethesda, Maryland 20014

Canick, Paul M.

Collins Radio Co.
Cedar Rapids, Iowa 52406

Bergemann, Gerald T.
Loupee, Burton J.

Collins Radio Co.
Dallas, Texas 75207

Cox, Robert T.
Eckert, James E.

Communications Satellite Corp.
1900 L Street, N. W.
Washington, D. C. 20036

Esch, Fred H.
Martin, Edward J.
Metzger, Sidney

Communications Systems, Inc.
Paramus, New Jersey

Dubbs, William M.
Kandoian, Armig G.
Lewinter, Sidney W.

Deco Electronics, Inc.
35 Cambridge Parkway
Cambridge, Massachusetts

Welti, George R.

Deco Electronics, Inc.
P.O. Box 551
Fort Evans Rd.
Leesburg, Virginia

Edmunds, Francis E.

Defense Communications Agency
Department of Defense
Washington, D.C. 20305

Herr, Clyde W.

Harry Diamond Labs.
Washington 25, D.C.

Salerno, James

Electronic Communications, Inc.
1501-72nd St., North
Box 12248
St. Petersburg, Florida 33733

Clark, Donald P.
Ellett, James T.
Ellington, Troy D.
LaVean, Gilbert E.

Fairchild-Hiller
Space Systems Division
1455 Research Blvd.
Rockville, Maryland

Hoyer, Sigurd
Kerr, John S.
Johnston, William A., Jr.

Federal Communications Commission
Washington, D.C. 20554

Skrivseth, Arnold G.

General Electric Company
Missile and Space Division
Valley Forge Space Technology Center
Goddard Blvd.
King of Prussia, Pennsylvania

Hagen, Donald L.
Skolka, Kenneth M.

General Electric Company
Defense Electronics Division
100 Plastics Ave.
Pittsfield, Massachusetts

Haaland, Kenneth E.

General Electric Company
Defense Programs Division
114 Waltham Street
Lexington, Massachusetts

McClennan, John H.

General Electric Company
6901 Elmwood Ave.
Philadelphia, Pennsylvania

Tenney, Raymond F.

Hazeltine Corporation
Little Neck, New York 11362

Dunn, Bradley B.
Regis, Robert

Hughes Aircraft Company
1901 W. Malvern
Fullerton, California

Golden, Edward
Hester, Robert G.
Honnold, Vincent R.
Sheridan, Edward W.

Hughes Aircraft Company
Florence Avenue at Teale
Culver City, California

Graves, Ross E.
Weltin, Otto K.

International Business Machines Corp.
7220 Wisconsin Ave.
Bethesda, Maryland

Blasbalg, Herman L.
Haddad, Raymond A.

ITT Federal Laboratories
500 Washington Ave.
Nutley, New Jersey 07110

Campbell, Donald R.
Lyon, Zeon G., Jr.
Walker, James L.

Lockheed Missiles and Space Company
P.O. Box 504
Sunnyvale, California

Briskin, Herbert B.
Edwards, Lawrence K.

LTV Aerospace Corporation
(A Subsidiary of Ling-Temco-Vought, Inc.)
9314 Jefferson Blvd.
P.O. Box 5907
Dallas, Texas 75222

Litton, Gail Thomas

Magnavox Research Laboratories
2829 Maricopa Street
Torrance, California 90503

Cahn, Charles R.
Judge, William J.
Masterson, Steven A.

Martin Company
P.O. Box 179
Denver, Colorado

Clausen, Reid H.
Hardin, Robert H.
Roberts, Alan F.

Martin Company
P.O Box 5837
Orlando, Florida

Koppel, Herbert
Prihar, David Y.

MITRE Corporation
P.O. Box 208
Bedford, Massachusetts

Desrosiers, Albert J.

Motorola, Inc.
Military Electronics Division
Western Center
8201 East McDowell Road
Scottsdale, Arizona

Engle, Kenneth J.
Estes, Charles L.
Krasin, Fred E.

Motorola, Inc.
Military Electronics Division
600 Main Street
Waltham, Massachusetts

Kendall, Percy R.

North American Aviation, Inc.
Space and Information Systems Div.
12214 Lakewood Blvd.
Downey, California 90241

Hathaway, Robert N.
Surrah, Gordon R.
Wehner, Gilbert L.

Ohio State University
1314 Kinnear Road
Columbus, Ohio 43212

Fouty, Robert A.
Long, Ronald K.
Zolnay, Stephen L.

Philco Corporation
WDL Division
3825 Fabian Way
Palo Alto, California

Bates, J. Fred
Davies, Richard S.
McClannan, Quinton B.

Radiation, Inc.
Box 37
Melbourne, Florida

Barkman, Richard D.
Seng, Frank G.
Sissom, Alton W.

Radop Corporation of America
Defense Electronic Products
Camden, New Jersey

Feller, J.
Solomon, K.

Radio Corporation of America
Defense Electronic Products
Moorestown, New Jersey

Bry, John C.
Johnston, Thomas M.
Sheridan, Thomas R.

Radio Corporation of America
Defense Electronic Products
Astro-Electronics Division
P.O. Box 800
Princeton, New Jersey

Miller, Bernard P.
Sherlock, Thomas M.
Silverman, Donald

Raytheon Company
1415 Boston-Providence Turnpike
Norwood, Massachusetts

Bickford, William J.
Pontecorvo, Paul J.
Tsao, Carson K.H.

Raytheon Company
Space and Information Systems Div.
528 Boston Post Road
Sudbury, Massachusetts 01776

Gicca, Francis A.
Trask, David B.

Sanders Associates, Inc.
95 Canal Street
Nashua, New Hampshire 03060

Cullen, Francis P.
Kingman, Gordon M.

Sylvania Electric Products, Inc.
Wehrle Drive and Cayuga Road
Williamsville, New York 14221

Diab, Khaled M.
Gray, Donald J.
Hyams, Henry C.
Schlichter, Ernest S.

System Sciences Corporation
5718 Columbia Pike
Falls Church, Virginia 22041

Burgess, John L.
Cerva, Calvin H.
Fruchter, Charles L
Marsh, Edward N.
Maxwell, David J.

Technical Communications Corp.
442 Marrett Road
Lexington, Massachusetts 02173

Dayton, David S.
Griffiths, Andrew S.
Smith, William H.

TRW Systems
One Space Park
Redondo Beach, California 90278

Littenberg, William

Westinghouse Electric Corp.
Defense and Space Center
Friendship International Airport
Baltimore, Maryland 21203

Mongold, Guy E.
Mueller, Edward J.
Robbins, Manuel A.

Whittaker Corporation
9229 Sunset Boulevard
Los Angeles, California 90069

Cluster, Alvin P.

USASCA
U.S. Army Satellite Comm. Agency
Fort Monmouth, New Jersey 07703

Chewey, Vincent C.

HQ. USAF

Lt. Colonel H. A. Wilkes, USAF
AFRDD
Headquarters United States Air Force
Washington, D. C. 20330

ODDR+E

Colonel Arthur W. Reese, USAF
Office of Secretary of Defense
Office of Director of Defense
Research and Engineering
Washington, D. C. 20301

RTD

Mr. David Anderson
Headquarters Research and
Technology Division (RTTC)
Bolling Air Force Base, D. C. 20332

NAVY

LCDR William R. Coffman, USN
OPNAV
Department of the Navy
Washington, D. C. 20350

Naval Security Group Headquarters
3801 Nebraska Avenue
Washington, D. C.

LCDR Angus D. McEachen, USN

NAVY

Mr. John M. Comiskey
U.S. Navy Underwater Sound
Laboratory
Fort Trumbull
New London, Connecticut 06321

Department of the Navy
Bureau of Naval Weapons
Washington, D. C. 20360

Mr. Richard T. Shearer
Cdr. Harold R. Gordinier, USN

Naval Electronics Systems Command
5805 Leesburg Pike
Bailey's Crossroads, Virginia 22041

Mr. Mario J. Amico
Mr. Joseph Awramik, Jr.
Mr. Joseph J. Bogart
Mr. Norman Horowitz
Mr. Kenneth L. Nichols
Mr. Harry M. Yakabe

Naval Communication Systems Hdqtrs.
5827 Columbia Pike
Bailey's Crossroads, Virginia

Lt. Donald C. Gibson, USN

U.S. Naval Research Laboratory
Washington, D. C. 20390

Mr. Theodore J. Altman
Mr. Herman J. Wirth
Mr. Robert W. Zeek

Cdr. A.K. Blough
Department of the Navy
Bureau of Ships
Code 670G
Washington, D. C.

DOCUMENT CONTROL DATA – R&D

(Security classification of title, body of abstract and indexing annotation must be entered when the overall report is classified)

1. ORIGINATING ACTIVITY *(Corporate author)* Lincoln Laboratory, M.I.T.	2a. REPORT SECURITY CLASSIFICATION Unclassified 2b. GROUP None

3. REPORT TITLE

Noise Temperature of Airborne Antennas at UHF

4. DESCRIPTIVE NOTES *(Type of report and inclusive dates)*

Technical Note

5. AUTHOR(S) *(Last name, first name, initial)*

Ploussios, George

6. REPORT DATE	7a. TOTAL NO. OF PAGES	7b. NO. OF REFS
6 December 1966	62	14

8a. CONTRACT OR GRANT NO. AF 19(628)-5167 b. PROJECT NO. 649L c. d.	9a. ORIGINATOR'S REPORT NUMBER(S) Technical Note 1966-59 9b. OTHER REPORT NO(S) *(Any other numbers that may be assigned this report)* ESD-TR-66-237

10. AVAILABILITY/LIMITATION NOTICES

Distribution of this document is unlimited.

11. SUPPLEMENTARY NOTES	12. SPONSORING MILITARY ACTIVITY
None	Air Force Systems Command, USAF

13. ABSTRACT

Partial results of an experimental program to determine the electromagnetic noise environment at UHF on board an aircraft are presented. Contributors to an airborne receiver noise temperature including galactic noise, earth temperature, P-static, atmospherics and industrial noise were measured and are discussed. A model of the industrial noise is presented whereby the industrial area is considered as a uniformly distributed source of independent radiators, the magnitude being the same for all cities measured with the exception of the New York City area.

RFI generated by on-board equipment and/or ground transmitters will be covered in a subsequent report.

14. KEY WORDS

airborne antennas
airborne receiver noise temperature
UHF antennas
galactic noise
thermal earth radiation
precipitation static
atmospherics
industrial noise
electromagnetic radiation